VARIATIONAL STUDY OF INTERACTING SU-SCHRIEFFER-HEEGER MODEL

A THESIS SUBMITTED TO
THE GRADUATE SCHOOL OF ENGINEERING AND SCIENCE
OF BILKENT UNIVERSITY
IN PARTIAL FULFILLMENT OF THE REQUIREMENTS FOR
THE DEGREE OF
MASTER OF SCIENCE
IN
PHYSICS

By
Luqman Saleem
September 2018

Variational study of interacting Su-Schrieffer-Heeger model
By Luqman Saleem
September 2018

We certify that we have read this thesis and that in our opinion it is fully adequate, in scope and in quality, as a thesis for the degree of Master of Science.

Balazs Hetényi(Advisor)

Bilal Tanatar

Seçkin Kürkcüoğlu

Approved for the Graduate School of Engineering and Science:

Ezhan Karaşan
Director of the Graduate School

ABSTRACT

VARIATIONAL STUDY OF INTERACTING SU-SCHRIEFFER-HEEGER MODEL

Luqman Saleem
M.S. in Physics
Advisor: Balazs Hetényi
September 2018

The interacting Su-Schrieffer-Heeger model with nearest neighbor interaction in one dimension at half-filling is studied. To obtain ground state wave function, the Baeriswyl variational wave function is extended to account for alternating hopping parameters. The ground state energy is numerically calculated and compared with exact diagonalization calculations, finding excellent agreement. Full phase diagram of the model is constructed which shows three different phases. When all hopping parameters are same the ideal metal-insulator phase transition is found at finite interaction, somewhat less than the exact results. The conducting phase is a Fermi sea. The phase transitions found are first order. With alternating hopping parameters the small interaction phase is the ground state of the Su-Schrieffer-Heeger model and the large interactions phase is an insulator. The phase transition has been visualized by constructing the parent Hamiltonian of the ground state wave function and tracing out the curves of the Brillouin zone. The polarization distribution is reconstructed from its cumulants on two different paths taken in the parametric space of interaction and hopping parameter. The first path is taken as it crosses the metallic phase line while the other path makes a semi-ellipse avoiding the metallic line. In the former case, the distribution is centered at one site and discontinuously jumps to the next site after crossing the metallic phase line, while in latter case distribution walks smoothly from one site to the next. These results suggest that interaction breaks the chiral symmetry of the Su-Schrieffer-Heeger model, in the same way as on-site potential breaks it in Rice-Mele model.

Keywords: Phase transition, lattice models, variational techniques, many-body condensed matter approximation, Baeriswyl wave function, electric polarization, Berry phase.

ÖZET

ETKILEşEN SU-SCHRIEFFER-HEEGER MODELIN VARYASYONEL ÇALıŞMASı

Luqman Saleem
Fizik, Yüksek Lisans
Tez Danışmanı: Balazs Hetényi
Eylül 2018

Bir boyutta, yarı doldurulmuş, en yakın komşu etkileşimini göz önünde bulunduran, etkileşen Su-Schrieffer-Heeger modeli çalışıldı. Temel durum dalga fonksiyonunu elde etmek için, Baeriswyl varyasyonel dalga fonksiyonu değişen sıçrayış parametrelerini ifade etmek için genelleştirildi. Temel durum enerjisi sayısal olarak hesaplandı ve gerçek diyagonalizasyon hesapları ile kıyaslandı; sonucunda son derece iyi eşleşme bulundu. Üç farklı fazı gösteren bahsi geçen modelin tam faz diyagramı yapıldı. Tüm sıçrayış parametleri aynı olduğunda, sonlu etkileşimde ideal metal-yalıtkan faz geçişi bulundu ve bu değer ,bir şekilde , kesin sonuçtan daha az bulundu. İletken faz Fermi denizidir. Bulunan faz geçişleri birinci derecedendir. Değişen sıçrayış parametreli dar ve geniş etkileşim fazları sırasıyla Su-Schrieffer-Heeger modelin temel durumu ve yalıtkandır. Faz geçişi temel dalga fonksiyonunun benzer Hamiltonian'ı kullanılarak ve Brillouin alanındaki eğriler bulunarak görselleştirildi. Polarizasyon dağılımı ,çizgilerin etkileşimin parametrik uzayında ve sıçrayış parametresinde olduğu, iki farklı çizginin kümülatifi alınarak yeniden yapıldı. İlk çizgi metalik faz çizgisini kesecek şekilde alınırken ikinci çizgi ise eliptik bir güzergaha sahip olacak ve metalik çizgiden uzak duracak şekilde seçildi. Bu durumların ilkinde dağılım bir konumum merkezine yerleşti, ve süreksiz bir şekilde, metalik faz çizgisini kestikten sonra, bir sonraki konuma sıçradı; durumlardan ikincisinde, dağılım bir konumdan ötekine yavaş ve sakin bir şekilde yürüdü. Bu sonuçlar gösteriyor ki etkileşim Su Schrieffer-Heeger modelin Chiral simetrisini bozmaktadır, aynı şekilde, konum üzerindeki potensitel, Rice-Mele modelin simetrisini bozmaktadadır.

Anahtar sözcükler: Faz geçişi, örgü modeli, varyasyonel teknikler, çoklu parçacık yoğun madde fiziği, Baeriswyl dalga fonksiyonu, elektriksel polarizasyon, Berry fazı.

Dedicated to my parents $\cdots$

Acknowledgement

I am extremely thankful to my parents, Muhammad Saleem and Razia Bibi for supporting my decisions and believing in me while I didn't. They have a huge role in any achievement that I have made. From my birth to this masters thesis, they always helped me by giving their precious love and support. I am also thankful to my brothers and sister for their priceless love. Their love made me feel like they were with me during my graduate years even though they were physically thousands of kilometers away from me.

I am also very thankful to my thesis advisor Asst. Prof. Dr. Balazs Hetényi of the Department of Physics at Bilkent University for helping me with this research work. Prof. Hetényi always answered all my questions with patience, even though sometimes my questions were very stupid.

I acknowledge Mohammad Yahyavi and Sina Gholizadeh, Ph.D. students of Prof. Hetényi who helped me during this research as friends and colleagues. I also acknowledge Muhammad Hilal, an MS Physics student at Bilkent University for our meaningful discussions about this research work.

I would like to acknowledge my dear friends Sabeeh Iqbal, Ali Sheraz, Farhan Ali, Ibn-e-Abbas, Zahid Ali, Ayyaz Ahmad and Shbahit Ali who always kept me motivated to complete this research work. Finally, I am very thankful to Hamdi Burak Bayrak, an MS student at Bilkent University who translated the abstract of this thesis into Turkish.

Luqman Saleem

Contents

List of Figures

List of Tables

Chapter 1

Introduction

For a long time, Landau theory has been used to describe all phases of matter. Physicists believed that all phases of matter can be explained by symmetries of the ground-state of the system. But in 1975, the discovery of the integer quantum Hall effect made it clear that not all possible phases of matter can be explained using Landau theory. A new type of phases was introduced named "Topological phase of matter". Since then this field has been one of the most active areas of research. Recent efforts have been mainly focused on understanding the effect of interaction between the particles on the topology of the system. The Kane-Mele-Hubbard (KMH) model [1] has received considerable attention in this regard, both analytically [2, 3] and numerically [4, 5].

In this thesis, we first study the spinless Su-Schrieffer-Heeger (SSH) [6] model on a one-dimensional half-filled lattice with nearest neighbor interaction using a variational wave function. The SSH model was first introduced in 1979 to study solitons in polyacetylene. It is a one-dimensional lattice model with alternating nearest-neighbor hopping. Despite its simplicity, this model exhibit very interesting physics: topological character, charge fractionalization [7, 8]. It has two different phases, one has trivial topology while the other has non-trivial topological protected conducting edge states on the ends of the chain. Although this model has received a lot of attention there is still a need to study the effect of interaction on this model.

Variational wave functions are very important in condensed-matter physics, for example, Yosida, BCS and Gutzwiller variational wave functions [9, 10] are used to study the Kondo model [11], superconductivity and the Hubbard model[12] respectively. The bosonic version of Gutzwiller wave function (GWF) was used to study the dynamics in the Bose-Hubbard model [13]. Also, the Gutzwiller approximation is used to study fermionic version of the Hubbard model for its time evaluation[9, 10]. Moreover, the variational wave functions have been merged with computational methods like Monte Carlo to evaluate the system with a large number of parameters [14, 15]. A well-chosen value of variational parameters for this kind of wave functions can provide vital information of complex many-body systems.

The standard way to construct the GWF is to take a completely delocalized state and apply an interaction depended operator on it which projects out the states that are not favorable for the interaction (i.e. doubly occupied states for spinful fermionic systems and states with the nearest neighbor (NN) filled sites for spinless fermionic systems with only NN interaction). There is a completely opposite approach to construct variational wave functions; the Baeriswyl wave function (BWF). BWF starts from the fully localized state on which kinetic energy dependent operator is applied which promotes the effect of particle' hopping between sites. In both above-mentioned wave functions, applied projectors depend upon the variational parameter i.e. strength of projectors is the variational parameter.

We extend BWF to account for alternating hopping in the SSH model, calculate ground-state energies for different parameters and compare them with exact diagonalization (ED) calculations, finding excellent agreement. We calculate the phase diagram of the full interacting SSH model which is outstandingly similar to the phase diagram of the KMH model. The phase transitions we found are first order. The phase diagram was quite interesting because for the interacting system we found a metal-insulator transition at $V = 1.3365\ldots$, which is less than the exact solution result ($V = 2$). When hopping between all NN sites become homogeneous we get a conducting phase (a Fermi sea in this variational approach) for small interactions, for large interactions we get a correlated insulator which has charge density wave (CDW) ordering. With alternating hopping, we get an

SSH ground-state for small interactions but an increase in interaction pushes the system toward a CDW ordered insulator. Also, to visualize the phase transition we construct the parent Hamiltonian of the BWF and calculate curves traced out by k-vector across the Brillouin zone.

We then study the polarization distribution of interacting SSH model. Usually, in any analysis of topological behavior, the Berry phase [16] is the starting point. The Berry phase is a phase which is picked up by any state when it is circled in a parametric space of the system. This phase arises due to the geometry of the space. When the ground-state of the condensed matter system is circled across the Brillouin zone, this phase is known as the Zak phase [17]. The polarization of a crystalline system is directly related the Zak phase. The Zak phase can also be taken as the first term in a series of gauge invariant cumulants[18, 19, 20]. The second term is the variance in the center of mass of the electronic charge distribution. The third cumulant, also known as the skewness of the distribution, is related to the second-order nonlinear optical response.

We calculate cumulants and reconstruct the distribution using the first three cumulants. We take two paths in the parametric space of the system, both connect two different topological states. The first path that is taken at the constant value of interaction, it crosses the metallic phase line, the second path makes a semi-ellipse in space avoiding metallic phase line. On the first path, mean of distribution remains constant on $x = -0.5$ until the metallic phase line is crossed, after that distribution is suddenly shifted to a new point $x = +0.5$ and remains there for the rest of the path. This sudden jump shows that one unit of charge is pumped suddenly from one site to the next [21]. In contrast to the first path, on the second path the mean of the polarization changes smoothly from $x = -0.5$ to $x = +0.5$.

To analyze these results, we compare them with a well-known topological model, the Rice-Mele (RM) model [22], which is defined as the SSH model plus alternating on-site potential. The SSH model has the chiral symmetry which gives rise to symmetry protected topological phases separated by the topological non-trivial point. The on-site potential breaks this chiral symmetry. We again take two paths in the parametric space of the RM model, both connecting two distinct topological states and construct distribution. On the first path, chiral symmetry

is always respected while on the second path symmetries are relaxed. We find that polarization distribution changes exactly in the same manner.

The rest of the thesis is organized as follows. In chapter 2 SSH, RM and interacting SSH models are discussed. In chapter 3 ED calculations, BWF and the ground-state energy of the BWF are derived. Chapter 4 addresses the Zak phase, the modern theory of polarization, cumulants and reconstruction of the probability distribution. We present our results in chapter 5 and finish thesis with a comprehensive conclusion in chapter 6.

Chapter 2

Model

To study the effect of interaction on polarization we need to take a model which has non-zero polarization without interaction. We take a well celebrated topological model, Su-Schrieffer-Heeger (SSH), which has very interesting properties in view of topological insulators. In this chapter, we will start from the discussion of the simple SSH model in different formalisms which will be followed by its study with and without on-site potential and at the end we will introduce the nearest neighbor (NN) interaction on it.

2.1 The Su-Schrieffer-Heeger model

The SSH model was first introduced by W. P. Su *et. al.* in 1979 to describe solitons in polyacetylene [6]. In recent times, it attracted attention of many researchers because of its interesting topological properties, non-trivial edge states and fractional charge [23, 24, 8, 7, 25, 26]. We consider spinless fermions on a one-dimensional (1D) lattice with alternating hopping strengths at half-filling. This staggered hopping in SSH is found naturally in various condensed matter systems, this is also known as a Peierls instability[27]. The lattice Hamiltonian,

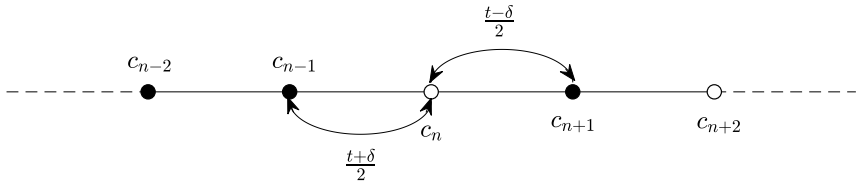

(a)

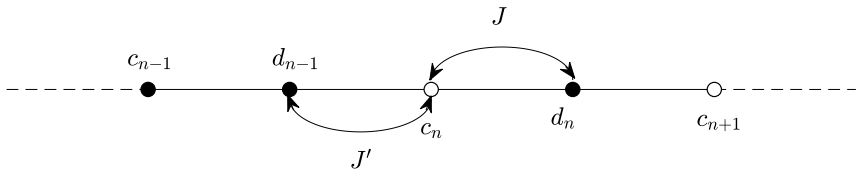

(b)

Figure 2.1: (a) Schematic of SSH model. t is average hopping and δ is deviation of hopping. Solid circles show filled sites while open represent empty sites., (b) Schematic of SSH model written in J and J' parameters

in second quantization [28], can be written as follow

$$H_0 \equiv H_{SSH} = -\frac{1}{2}\sum_{n=1}^{L}\left[t+\delta(-1)^n\right]c_n^\dagger c_{n+1} + h.c. \tag{2.1}$$

where $c_i^\dagger(c_i)$ creates (annihilates) a particle on site i, L is the total number of sites in the chain, t is the average hopping strength, δ is the deviation of the hopping strength between NN sites i.e. between even (odd) bond hopping strength is $t+\delta(t-\delta)$ and $h.c.$ is the Hermitian conjugate. A schematic is shown in Figure. 2.1(a).

Creation and annihilation operators obey the following anti-commutation relations that make system obey Pauli's principle automatically:

$$\{c_i^\dagger, c_j\} = \delta_{i,j} \tag{2.2a}$$

$$\{c_i^\dagger, c_j^\dagger\} = 0 \tag{2.2b}$$

$$\{c_i, c_j\} = 0 \tag{2.2c}$$

here $\{X, Y\} = XY + YX$. In second quantization $|0\rangle$ is considered as the fermionic vacuum. Creation and annihilation operators act as following:

$$c_n^\dagger|0\rangle = |n\rangle$$
$$c_n|n\rangle = |0\rangle$$
$$c_n|0\rangle = c_n^\dagger|n\rangle = 0$$

To easily diagonalize (2.1), one can introduce new set of basis $[c_i, d_i]$ and write Hamiltonian as following

$$H_0 = -J\sum_{n=1} c_n^\dagger d_n - J'\sum_{n=1} d_n^\dagger c_{n+1} + h.c. \tag{2.3}$$

Where $d_n^\dagger(d_n)$ is creates (annihilates) particle on site n and

$$J = (t+\delta)/2 \tag{2.4a}$$
$$J' = (t-\delta)/2 \tag{2.4b}$$

This is depicted in Figure. 2.1(b). It is easier to diagonalize H_0 to find ground-state energy and wave function by converting (2.3) into Fourier space and using the Bloch theorem [29]. The Fourier transformation of the creation(annihilation) operator can be written as

$$c_n = \frac{1}{\sqrt{L}}\sum_k \exp(-ikn)c_k \tag{2.5a}$$
$$c_n^\dagger = \frac{1}{\sqrt{L}}\sum_k \exp(ikn)c_k^\dagger \tag{2.5b}$$

Here, k is wave vector. When $J = J'$, the lattice is periodic with a unit-cell of one site per cell so k is well defined in region $(-\pi, \pi)$. For $J \neq J'$, due to the Peierls instability periodicity become two sites per unit-cell which makes the k vector defined in region $(-\pi/2, \pi/2)$. The spacing between k points is $2\pi/L$ and π/L for $J = J'$ and $J \neq J'$ case respectively. L is always even in these calculations. The following important identity can be derived from (2.5)[29]

$$\frac{1}{L}\sum_n \exp[\pm i(k-k')n] = \delta_{k,k'} \tag{2.6}$$

Performing the Fourier transformation on the first term of (2.3) gives

$$\begin{aligned} -J\frac{1}{L}\sum_{n}\sum_{k,k'} e^{ikn}e^{-ik'(n+1)}c_k^\dagger d_{k'} &= -J\sum_{k,k'}\frac{1}{L}\sum_{n} e^{i(k-k')n}e^{-ik'}c_k^\dagger d_{k'} \\ &= -J\sum_{k} e^{ik}c_k^\dagger d_k \end{aligned} \tag{2.7}$$

Where in the second step we have used (2.6). Similarly, the second term of (2.3) yield following

$$-J'\sum_{k}\exp(ik)d_k^\dagger c_k \tag{2.8}$$

Complete Hamiltonian in Fourier space become

$$\begin{aligned} \tilde{H}_0 &= \sum_k \big[-Je^{ik} - J'e^{-ik}\big]c_k^\dagger d_k + \sum_k \big[-Je^{-ik} - J'e^{ik}\big]d_k^\dagger c_k \\ \tilde{H}_0 &= \begin{bmatrix} c_k^\dagger & d_k^\dagger \end{bmatrix}\begin{bmatrix} 0 & -Je^{ik} - J'e^{-ik} \\ -Je^{-ik} - J'e^{ik} & 0 \end{bmatrix}\begin{bmatrix} c_k \\ d_k \end{bmatrix} \end{aligned} \tag{2.9}$$

Now we have to find eigenstates and eigenvalues of a 2-by-2 matrix for ground-state energy and wave function. Using the Pauli matrix, this two-level system can be represented as

$$\tilde{H}_0 = \mathbf{h(k)}\cdot\sigma = h_x\sigma_x + h_y\sigma_y + h_z\sigma_z \tag{2.10}$$

Here σ_i are Pauli matrices and

$$h_x = -(J + J')\cos(k) \tag{2.11a}$$

$$h_y = -(J - J')\sin(k) \tag{2.11b}$$

$$h_z = 0 \tag{2.11c}$$

Eigenstates of any system written in (2.10) form are [30]

$$|E_+\rangle = \begin{bmatrix} \cos(\theta/2) \\ e^{-i\phi}\sin(\theta/2) \end{bmatrix}; \qquad |E_-\rangle = \begin{bmatrix} \sin(\theta/2) \\ e^{-i\phi}\cos(\theta/2) \end{bmatrix} \tag{2.12}$$

Here $|E_-\rangle$ is ground-state and θ and ϕ are defined as [30]

$$\cos\theta = \frac{h_z}{|\mathbf{h(k)}|}; \qquad e^{i\phi} = \frac{h_x + ih_y}{\sqrt{h_x^2 + h_y^2}} \tag{2.13}$$

$|\mathbf{h(k)}|$ being magnitude of $\tilde{H}_0$ i.e. $|\mathbf{h(k)}| = \sqrt{h_x^2 + h_y^2 + h_z^2}$. By putting (2.11) in (2.13), we get

$$\theta = \pi/2; \qquad \phi = \tan^{-1}\left[\frac{(J - J')\sin(k)}{(J + J')\cos(k)}\right] \tag{2.14}$$

Hence we have successfully found the ground-state wave function of the simple SSH model.

2.1.1 Few properties of SSH model

The SSH model has chiral symmetry and it is metallic when $J = J'$ ($\delta = 0$) and insulator otherwise [30]. The energy dispersion relation of SSH model can be derived from (2.10)

$$E(k) = \sqrt{h_x^2 + h_y^2 + h_z^2} = \sqrt{(J + J')^2 \cos^2 k + (J - J')^2 \sin^2 k} \tag{2.15}$$

For different values of J and J' dispersion relation is plotted in Figure. 2.2. It can be seen that a gap closes at one point and then it re-opens. For $J > J'$ and $J < J'$, dispersion plots are the same but they have different topology i.e. the Zak phase, which is equal to first cumulant of itself, [17] changes from $-\pi/2$ to $\pi/2$. Details of Zak phase are given in Chapter 4 and calculated cumulants are given in Chapter 5. Pseudo-spin representation of vector $\tilde{H}_0$ is also shown in Figure. 2.2. Different spin direction indicates different distinct topologies separated by topological phase transition point $J = J'$ or $\delta = 0$.

In the next section, we will study the SSH model with an on-site potential.

2.2 The SSH model with on-site potential

The SSH model with alternating on-site potential is known as the Rice-Mele (RM) model [22], this alternating on-site potential breaks the chiral symmetry of the SSH model [30]. The On-site potential can be written in second quantized form

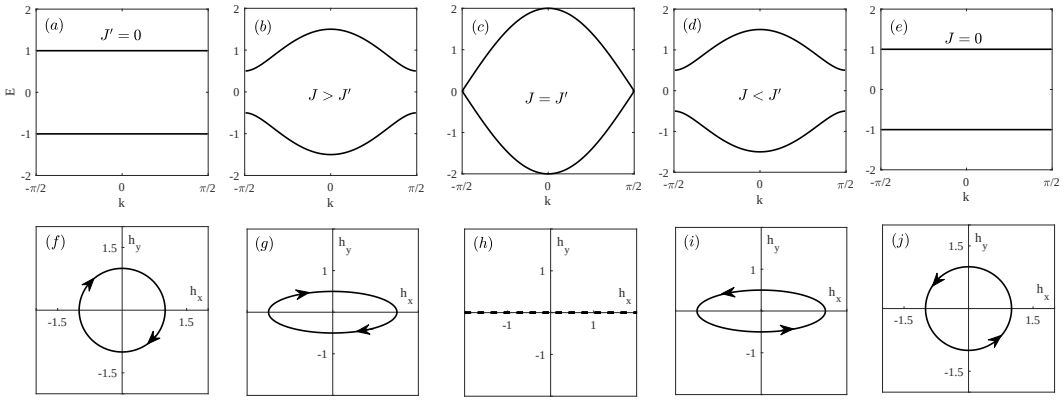

Figure 2.2: Energy dispersion plots of SSH model for different values of J and J'. (a) $J = 1, J' = 0$, (b) $J = 1, J' = 0.5$, (c) $J = 1, J' = 1$, (d) $J = 0.5, J' = 1$ and (e) $J = 0, J' = 1$. For each case, pseudo-spin representation of $\tilde{H}_0$ vector is also plotted on h_x and h_y plane.

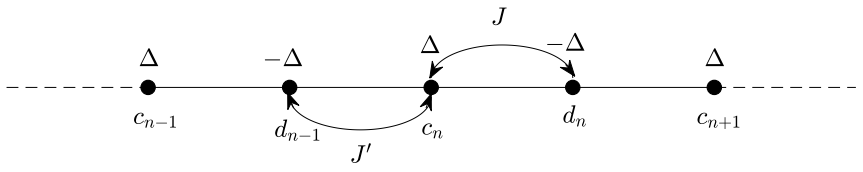

Figure 2.3: Schematic of the SSH model with on-site potential

as follows

$$H_\Delta = \Delta \sum_n^L \left[c_n^\dagger c_n - d_n^\dagger d_n\right] \tag{2.16}$$

Where Δ is the strength of on-site potential. This model is depicted in Figure.2.3.

In Fourier space H_Δ become

$$\tilde{H}_\Delta = \Delta \sum_{k,k'} \sum_n^L \frac{1}{L} e^{in(k-k')} \left[c_k^\dagger c_{k'} - d_k^\dagger d_{k'}\right] = \Delta \sum_k [c_k^\dagger c_k - d_k^\dagger d_k] \tag{2.17}$$

Total Hamiltonian of RM is $H_{on-site} = H_0 + H_\Delta$

$$\tilde{H}_{on-site} = \begin{bmatrix} c_k^\dagger & d_k^\dagger \end{bmatrix} \begin{bmatrix} \Delta & -Je^{ik} - J'e^{-ik} \\ -Je^{-ik} - J'e^{ik} & -\Delta \end{bmatrix} \begin{bmatrix} c_k \\ d_k \end{bmatrix}$$

$$\tilde{H}_{on-site} = h_x\sigma_x + h_y\sigma_y + h_z\sigma_z \tag{2.18}$$

with h_x and h_y given by 2.11 and $h_z = \Delta$. The ground-state wave function is given by 2.12 with ϕ given by (2.14) and

$$\theta = \tan^{-1}\left[\frac{|Je^{ik} + J'e^{-ik}|}{\Delta}\right] \tag{2.19}$$

Now the Zak phase can vary between $-\pi$ and π for different values of Δ [20].

2.3 The SSH model with NN interaction

The NN repulsive interaction V means that there will be extra V energy if two NN sites are occupied. It can be written in second quantized form as follows

$$H_{int} = V\sum_{n=1}^{L}\hat{n}_n\hat{n}_{n+1} \tag{2.20}$$

Where $\hat{n}_n = c_n^\dagger c_n$ is density operator which measures number of particle at site n. This model is depicted in Figure.2.4. Total Hamiltonian for interacting SSH model is sum of (2.1) and (2.20) i.e.

$$H = H_0 + H_{int} \tag{2.21}$$

For the interacting SSH it is convenient to use (2.1) as the definition of the SSH model. The Fourier transform of the first term of (2.1) is

$$-\frac{t}{2}\sum_k e^{-ik}c_k^\dagger c_k$$

and for second term, note that Fourier transform of $(-1)^n$ is $e^{i\pi n}$

$$-\frac{\delta}{2L}\sum_n\sum_{k,k'} e^{in(k-k'+\pi)}e^{-ik'}c_k^\dagger c_{k'} = \frac{\delta}{2}\sum_k e^{-ik}c_k^\dagger c_{k+\pi}$$

As it is non-zero only when $k' = k + \pi$. So, in Fourier space (2.1) become

$$\tilde{H}_0 = -\frac{t}{2}\sum_k e^{-ik}c_k^\dagger c_k + \frac{\delta}{2}\sum_k e^{-ik}c_k^\dagger c_{k+\pi} + h.c. \tag{2.22}$$

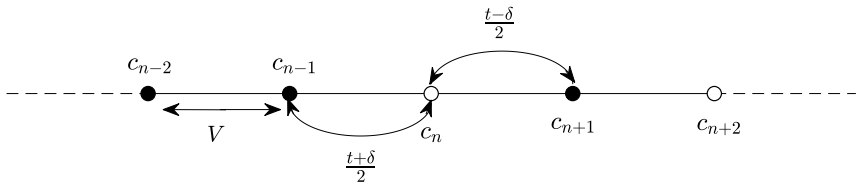

Figure 2.4: Schematic of interacting SSH model

To make this Hamiltonian Hermitian we can change limits of k from $(-\pi, \pi)$ to $(-\pi/2, \pi/2)$ i.e.

$$\begin{aligned}\tilde{H}_0 = \sum_{k=-\pi/2}^{\pi/2} \big[&- \frac{t}{2} e^{-ik} c_k^\dagger c_k + \frac{\delta}{2} e^{-ik} c_k^\dagger c_{k+\pi} - \frac{t}{2} e^{-i(k+\pi)} c_{k+\pi}^\dagger c_{k+\pi} \\ &+ \frac{\delta}{2} e^{-i(k+\pi)} c_{k+\pi}^\dagger c_{k+2\pi} \big] + h.c. \\ \tilde{H}_0 = \sum_k \big[&\epsilon(k) c_k^\dagger c_k - \epsilon(k) c_{k+\pi}^\dagger c_{k+\pi} + i\rho(k) c_k^\dagger c_{k+\pi} - i\rho(k) c_{k+\pi}^\dagger c_k \big] \end{aligned} \tag{2.23}$$

Where $\epsilon(k) = -\cos(k)$ and $\rho(k) = -\delta \sin(k)$ and $t = 1$. The Fourier transform of (2.20) can be performed as following

$$\begin{aligned}\tilde{H}_{int} &= \frac{V}{L^2} \sum_n \sum_{k,k',k'',k'''} e^{ikn} e^{-ik'n} e^{ik''(n+1)} e^{-ik'''(n+1)} c_k^\dagger c_{k'} c_{k''}^\dagger c_{k'''} \\ &= \frac{V}{L^2} \sum_n \sum_{k,k',k'',k'''} e^{in(k-k'+k''-k''')} e^{i(k''-k''')} c_k^\dagger c_{k'} c_{k''}^\dagger c_{k'''}\end{aligned}$$

This is non-zero only when $k - k' + k'' - k''' = 0$ or $k - k' = k''' - k'' = q$

$$\begin{aligned}\tilde{H}_{int} &= \frac{V}{L} \sum_{k,k',k'',k'''} e^{-iq} c_k^\dagger c_{k'} c_{k''}^\dagger c_{k'''} \\ \tilde{H}_{int} &= -\frac{V}{L} \sum_{k,k',q} \epsilon(q) c_{k+q}^\dagger c_k c_{k'-q}^\dagger c_{k'}\end{aligned} \tag{2.24}$$

Now, we cannot diagonalize (2.21) using Bloch states because of H_{int}. However, there are other methods to solve these types of Hamiltonians i.e. ED [31], the Bethe Ansatz (BA) [32], Density matrix renormalization group (DMRG) [33], Monte Carlo methods [34], Variational wave functions [9, 10, 13, 35] etc.

Chapter 3

Methods

In this chapter ED for interacting SSH model will be discussed. Unfortunately, ED cannot be performed for a large system size because the requirement of computer memory increases exponentially with system size. To overcome this problem, a variational wave function will be derived. In quantum mechanics, the variational wave function is a trial wave function which gives an approximation to the ground-state energy and its wave function. At the end of this chapter, exact terms for variational energy will also be calculated.

3.1 Exact diagonalization for the interacting SSH

For simplicity a system of 4 sites with periodic boundary conditions will be discussed. The main purpose is to find the ground-state energy. It is done by the representing Hamiltonian in the computer using matrices and finding its eigenvalues. The smallest eigenvalue is the ground-state energy. Ingredients for ED are

no.	algebraic	picture	binary	decimal
1	$c_3^\dagger c_4^\dagger \|0\rangle$	□□■■	$\|0011\rangle$	$\|3\rangle$
2	$c_2^\dagger c_4^\dagger \|0\rangle$	□■□■	$\|0101\rangle$	$\|5\rangle$
3	$c_2^\dagger c_3^\dagger \|0\rangle$	□■■□	$\|0110\rangle$	$\|6\rangle$
4	$c_1^\dagger c_4^\dagger \|0\rangle$	■□□■	$\|1001\rangle$	$\|9\rangle$
5	$c_1^\dagger c_3^\dagger \|0\rangle$	■□■□	$\|1010\rangle$	$\|10\rangle$
6	$c_1^\dagger c_2^\dagger \|0\rangle$	■■□□	$\|1100\rangle$	$\|12\rangle$

Table 3.1: Representation of basis in the computer for four sites at half-filling. Blank (filled) square show empty (occupied) sites. Binary digits can be converted into decimal digits to easily denote and use in computer programs

1. Hilbert space, basis representation
2. Hamiltonian Matrix
3. Linear Algebra packages i.e. LAPACK for finding eigenvalues

All basis states of Hilbert space have to be represented in the language of the computer. The easiest way is to represent it by binary digits i.e. 1 represents a filled site while 0 shows empty site. For 4 sites at half-filling, a basis set is given in Table 3.1. Using simple quantum mechanics, we can write Hamiltonian in matrix form as

$$H_0 \doteq \langle s|H_0|r\rangle \tag{3.1}$$

where $|i\rangle$ are basis vectors. Hamiltonian H_0 of interacting SSH model in second quantization is given by (2.21). For $L = 4$

$$H_0 = -\begin{bmatrix} c_1^\dagger & c_2^\dagger & c_3^\dagger & c_4^\dagger \end{bmatrix} \begin{bmatrix} 0 & t-\delta & 0 & t+\delta \\ t-\delta & 0 & t+\delta & 0 \\ 0 & t+\delta & 0 & t-\delta \\ t+\delta & 0 & t-\delta & 0 \end{bmatrix} \begin{bmatrix} c_1 \\ c_2 \\ c_3 \\ c_4 \end{bmatrix} \tag{3.2}$$

Explicitly writing (3.1) gives

$$H_0 = -\begin{bmatrix} \langle 3|H_0|3\rangle & \langle 3|H_0|5\rangle & \langle 3|H_0|6\rangle & \langle 3|H_0|9\rangle & \langle 3|H_0|10\rangle & \langle 3|H_0|12\rangle \\ \langle 5|H_0|3\rangle & \langle 5|H_0|5\rangle & \langle 5|H_0|6\rangle & \langle 5|H_0|9\rangle & \langle 5|H_0|10\rangle & \langle 5|H_0|12\rangle \\ \langle 6|H_0|3\rangle & \langle 6|H_0|5\rangle & \langle 6|H_0|6\rangle & \langle 6|H_0|9\rangle & \langle 6|H_0|10\rangle & \langle 6|H_0|12\rangle \\ \langle 9|H_0|3\rangle & \langle 9|H_0|5\rangle & \langle 9|H_0|6\rangle & \langle 9|H_0|9\rangle & \langle 9|H_0|10\rangle & \langle 9|H_0|12\rangle \\ \langle 10|H_0|3\rangle & \langle 10|H_0|5\rangle & \langle 10|H_0|6\rangle & \langle 10|H_0|9\rangle & \langle 10|H_0|10\rangle & \langle 10|H_0|12\rangle \\ \langle 12|H_0|3\rangle & \langle 12|H_0|5\rangle & \langle 12|H_0|6\rangle & \langle 12|H_0|9\rangle & \langle 12|H_0|10\rangle & \langle 12|H_0|12\rangle \end{bmatrix} \tag{3.3}$$

after putting (3.2) in (3.3) and solving the terms

$$H_0 = \begin{bmatrix} 0 & -t-\delta & 0 & 0 & t+\delta & 0 \\ -t-\delta & 0 & -t+\delta & -t+\delta & 0 & t+\delta \\ 0 & -t+\delta & 0 & 0 & -t+\delta & t+\delta \\ 0 & -t+\delta & 0 & 0 & -t+\delta & t+\delta \\ t+\delta & 0 & -t+\delta & -t+\delta & 0 & -t-\delta \\ 0 & t+\delta & 0 & 0 & -t-\delta & 0 \end{bmatrix} \tag{3.4}$$

The matrix of the interacting term is a diagonal matrix with non-zero values only if both NN sites are occupied. So total Hamiltonian of ED for 4 sites become

$$H_0 = \begin{bmatrix} V & -t-\delta & 0 & 0 & t+\delta & 0 \\ -t-\delta & 0 & -t+\delta & -t+\delta & 0 & t+\delta \\ 0 & -t+\delta & V & 0 & -t+\delta & t+\delta \\ 0 & -t+\delta & 0 & V & -t+\delta & t+\delta \\ t+\delta & 0 & -t+\delta & -t+\delta & 0 & -t-\delta \\ 0 & t+\delta & 0 & 0 & -t-\delta & V \end{bmatrix} \tag{3.5}$$

To find ground-state energy we have to find eigenvalues of above matrix using either MATLAB's *eig(), eigs()* function or *LAPACK* in FORTRAN. ED is a powerful tool to find the ground-state energy of many-body systems even though it has a strong system size limitation. The total number of basis vectors in Hilbert space increase exponentially with system size. Number of basis vectors with L site and N particles are given by $\frac{L!}{N!(L-N)!}$. For 10 and 20 sites at half-filling, dimensions of H_0 matrix are 252×252 and 184756×184756 respectively. This increase in the size of H_0 matrix makes ED impossible to be performed on large system sizes.

3.2 Variational principle of quantum mechanics

Let $|a\rangle$ be the complete orthonormal set of eigenstates of Hamiltonian H with eigen-energies $E_a \leq E_{a+1}$ where $a = 0, 1, 2, ...$ Any state $|\phi\rangle$ of system can be shown in the form

$$|\phi\rangle = \sum_a c_a |a\rangle \tag{3.6}$$

where c_a are coefficients of linear combination. The expectation value of energy is given as

$$E(\phi) = \frac{\langle\phi|H|\phi\rangle}{\langle\phi|\phi\rangle} \tag{3.7}$$

$$E(\phi) = \frac{\sum_a E_a |c_a|^2}{\sum_a |c_a|^2} \tag{3.8}$$

this fulfills the condition that $E(\phi)$ provides with upper bound of ground-state energy E_0 i.e. $E(\phi) \geq E_0$.

In the context of the variational scheme, we take a trial wave function $|\phi_t\rangle$ which depends on one or more than one variational parameters (α_i) and has desired symmetries. We find values of these variational parameters such that the energy of the system is minimum i.e.

$$\frac{\partial E(\phi_t)}{\partial \alpha_i} = 0 \tag{3.9}$$

this gives the best approximation of ground-state energy and wave function for the system.

It is difficult to say how close a variational wave function gives results to the exact ground-state. Sometimes ground-state energy is very close to exact results but corresponding wave function doesn't explain system truly. This can be because of degenerate energy states. An example can be the spinful Hubbard model with a large value of interaction V. Almost all states with large interaction have no doubly occupied sites which makes their energy equal. [36]

3.3 The Baeriswyl variational wave function

The Baeriswyl variational wave function (BWF) was first introduced by D. Baeriswyl in 1987 as a counterpart of the Gutzwiller wave funtion (GWF). The GWF explains very famous Mott-insulator transition but it fails at large value of the interaction V where BWF gives an excellent approximation.

Recipe of BWF:

The derivation of the BWF $|\psi_B\rangle$ starts from writing the state of the system in $V \to \infty$ limit ($|\psi_\infty\rangle$) and then applying variational parameter dependent kinetic energy operator on it i.e.

$$|\psi_B\rangle = N_B \exp(-\alpha \hat{H}_{kin})|\psi_\infty\rangle \tag{3.10}$$

where N_B is overall normalization factor and α is variational parameter. This operator promotes the hopping effect in the system.

For simplicity, we will first construct a BWF for simple spinless Hubbard model in 1D at half-filling and then follow the same procedure for interacting SSH model.

3.3.1 BWF for Hubbard model

The Hamiltonian of 1D spinless fermionic Hubbard model is given as

$$H = H_{kin} + H_{int} = -\frac{t}{2}\sum_{n=1}^{L} c_n^\dagger c_{n+1} + \frac{V}{2}\sum_{n=1}^{L} n_n n_{n+1} + h.c. \tag{3.11}$$

In Fourier space (3.11) becomes

$$\tilde{H}_{kin} = \sum_k \epsilon(k) c_k^\dagger c_k \tag{3.12a}$$

$$\tilde{H}_{int} = -\frac{V}{L}\sum_{k,k',q} \epsilon(q) c_{k+q}^\dagger c_k c_{k'-q}^\dagger c_{k'} \tag{3.12b}$$

where $\epsilon(k) = -\cos(k)$ and $t = 1$ is taken. As system is at half-filling in $V \to \infty$ limit there will be a CDW i.e. particle on every second site as shown in Figure. 3.1. $|\psi_\infty\rangle$ has a simple form in this case as follows

Figure 3.1: Charge density wave for a half-filled system. Blank (filled) circle show empty (occupied) sites and a is lattice constant.

$$|\psi_\infty\rangle = \prod_{k\epsilon RBZ} \frac{1}{\sqrt{2}}(c_k^\dagger + c_{k+Q}^\dagger)|0\rangle \tag{3.13}$$

where the product goes on reduced Brillouin zone (RBZ), $Q = \pi/a$ is ordering wave vector, a is lattice constant which is taken as one and $|0\rangle$ is a fermionic vacuum. After applying operator $\exp(-\alpha\tilde{H}_{kin})$ on (3.13) one can get BWF as following

$$|\psi_B\rangle = \prod_{k\epsilon RBZ} N_B\big[\exp(-\alpha\epsilon(k))c_k^\dagger + \exp(-\alpha\epsilon(k+\pi)c_{k+\pi}^\dagger)\big]|0\rangle$$

and normalization factor can be find by $\langle\psi_B|\psi_B\rangle = 1$. The final form of the wave function is

$$|\psi_B\rangle = \prod_{k\epsilon RBZ} \frac{\exp(-\alpha\epsilon(k))c_k^\dagger + \exp(\alpha\epsilon(k))c_{k+\pi}^\dagger}{\sqrt{2\cosh[2\alpha\epsilon(k)]}}|0\rangle \tag{3.14}$$

In Ref.[35] BWF was derived for 2D spinless Hubbard model. The above derived wave function is the exact counterpart of that wave function in 1D. This wave function gives a very good approximation of the ground-state energy as well as the wave function [35].

3.3.2 The BWF for the interacting SSH model

The Hamiltonian of the SSH is given by (2.23). Using Pauli matrices it can be written as

$$\tilde{H}_0 = \sum_k \begin{bmatrix} c_k^\dagger & c_{k+\pi}^\dagger \end{bmatrix} \begin{bmatrix} \epsilon(k) & i\rho(k) \\ -i\rho(k) & -\epsilon(k) \end{bmatrix} \begin{bmatrix} c_k \\ c_{k+\pi} \end{bmatrix} \tag{3.15}$$

$|\psi_\infty\rangle$ is given in (3.13) but now we cannot simply apply $\exp(-\alpha\tilde{H}_0)$ on this state because $\tilde{H}_0$ is not diagonalized in $[c_k^\dagger, c_{k+\pi}^\dagger]$ basis. To overcome this problem there are two ways

1. Diagonalize $\tilde{H}_0$ into some new basis let's say $[\beta_k^\dagger, \gamma_k^\dagger]$
2. Decompose exponential operator into even and odd terms

If we follow the first way and derive a wave function we will end up with 16 terms to be solved for the interaction part which will make this problem even more complicated. However, the second way can make this problem easier to solve. Using the Pauli matrices, we can write (3.15) as

$$\tilde{H} = \sum_k (h_x\sigma_x + h_x\sigma_y + h_x\sigma_z) \tag{3.16}$$

where $h_x = 0$, $h_y = \epsilon(k)$ and $h_z = -\rho(k)$ and σ_i are Pauli matrices. We can define a term $h(k)$ as

$$h(k) = \sqrt{h_x^2 + h_y^2 + h_z^2} \tag{3.17}$$

And operator $\exp(-\alpha\tilde{H}_0)$ can be expanded as

$$\begin{aligned}\exp(-\alpha\tilde{H}_0) &= \sum_{n=0}^{\infty} \frac{(-\alpha\tilde{H}_0)^n}{n!} \\ &= \sum_{n=0}^{\infty} \frac{\left[(-\alpha\tilde{H}_0)^2\right]^n}{(2n)!} + \sum_{n=0}^{\infty}(-\alpha\tilde{H}_0)\frac{\left[(-\alpha\tilde{H}_0)^2\right]^n}{(2n+1)!}\end{aligned} \tag{3.18}$$

Note that $\tilde{H}_0^2$ is

$$\begin{aligned}\tilde{H}_0^2 &= \tilde{H}_0 \cdot \tilde{H}_0 = (h_x\sigma_x + h_x\sigma_y + h_x\sigma_z)\cdot(h_x\sigma_x + h_x\sigma_y + h_x\sigma_z) \\ \tilde{H}_0^2 &= h_x^2 + h_y^2 + h_z^2 = h(k)^2\end{aligned} \tag{3.19}$$

we have used $\sigma_i^2 = I_2$, $\sigma_x\sigma_y + \sigma_y\sigma_x = \delta_{xy}I_2$ where $i = x, y, z$ while x, y, z are taken in a cycle and I_2 is 2-by-2 identity matrix. Put (3.19) in (3.18)

$$\begin{aligned}\exp(-\alpha\tilde{H}_0) &= \sum_{n=0}^{\infty} \frac{[\alpha h(k)]^{2n}}{(2n)!} I_2 - \alpha \sum_{n=0}^{\infty} \frac{[\alpha h(k)]^{2n}}{(2n+1)!}\tilde{H}_0 \\ \exp(-\alpha\tilde{H}_0) &= \cosh[\alpha h(k)] I_2 - \frac{\sinh[\alpha h(k)]}{h(k)}\tilde{H}_0\end{aligned} \tag{3.20}$$

in matrix form it can be written as

$$\exp(-\alpha\tilde{H}_0) = \begin{bmatrix} \cosh[\alpha h(k)] - \epsilon(k)\frac{\sinh[\alpha h(k)]}{h(k)} & -i\rho(k)\frac{\sinh[\alpha h(k)]}{h(k)} \\ i\rho(k)\frac{\sinh[\alpha h(k)]}{h(k)} & \cosh[\alpha h(k)] + \epsilon(k)\frac{\sinh[\alpha h(k)]}{h(k)} \end{bmatrix} \tag{3.21}$$

$|\psi_\infty\rangle$ from (3.13) can also be written in matrix form

$$|\psi_\infty\rangle = \prod_{k\epsilon RBZ} \frac{1}{\sqrt{2}} \begin{bmatrix} c_k^\dagger \\ c_{k+\pi}^\dagger \end{bmatrix} |0\rangle \tag{3.22}$$

Now, application of $\exp(-\alpha\tilde{H}_0)$ on $|\psi_B\rangle$ has become a simple multiplication. So, $|\psi_B\rangle$ becomes

$$|\psi_B\rangle = \prod_{k\epsilon RBZ} \frac{N_B}{\sqrt{2}} \Big[P(k)c_k^\dagger + P(k+\pi)c_{k+\pi}^\dagger \Big] |0\rangle \tag{3.23}$$

where $P(k) = \big[\cosh[\alpha h(k)] - \epsilon(k)\frac{\sinh[\alpha h(k)]}{h(k)} - i\rho(k)\frac{\sinh[\alpha h(k)]}{h(k)}\big]$ and N_B can be calculated using the normalization condition

$$\begin{aligned} 1 &= \sum_k \langle\psi_B|\psi_B\rangle \\ &= \sum_k \frac{N_B^2}{2} \langle 0| \big[P^*(k)c_k + P^*(k+\pi)c_{k+\pi}\big] \big[P(k)c_k^\dagger + P(k+\pi)c_{k+\pi}^\dagger\big] |0\rangle \\ &= \sum_k \frac{N_B^2}{2} \langle 0| \big[|P(k)|^2 c_k c_k^\dagger + P^*(k)P(k+\pi)c_k c_{k+\pi}^\dagger + P^*(k+\pi)P(k)c_{k+\pi}c_k^\dagger \\ &+ |P(k+\pi)|^2 c_{k+\pi}c_{k+\pi}^\dagger\big] |0\rangle \end{aligned} \tag{3.24}$$

Using $\{c_i, c_j^\dagger\} = \delta_{i,j}$ and the Wick's theorem [37] only the first and the last term will give non-zero results. After simplification, N_B can be written as follows

$$N_B = \sum_k \frac{\sqrt{2}}{\sqrt{2\cosh[2\alpha h(k)]}} \tag{3.25}$$

Putting (3.25) in (3.23) gives final form of wave function

$$|\psi_B\rangle = \prod_{k\epsilon RBZ} \Big[\chi(k)c_k^\dagger + \chi(k+\pi)c_{k+\pi}^\dagger \Big] |0\rangle \tag{3.26}$$

where

$$\chi(k) = \frac{\big[\cosh[\alpha h(k)] - \epsilon(k)\frac{\sinh[\alpha h(k)]}{h(k)} - i\rho(k)\frac{\sinh[\alpha h(k)]}{h(k)}\big]}{\sqrt{2\cosh[2\alpha h(k)]}}$$

In the next section, we will derive exact expectation values for kinetic and interaction energy.

3.4 Ground-state energy of BWF

The variational ground-state energy is found by minimizing it with respect to variational parameter α i.e. $E_0 = min_\alpha \langle\psi_B|\tilde{H}|\psi_B\rangle$. $\tilde{H}_0$ can be written as

$$\tilde{H}_0 = \sum_k \left[\epsilon(k)\left[c_k^\dagger c_k - c_{k+\pi}^\dagger c_{k+\pi}\right] + i\rho(k)\left[c_k^\dagger c_{k+\pi} - c_{k+\pi}^\dagger c_k\right]\right] \tag{3.27}$$

and its expectation values $\langle\tilde{H}_0\rangle$ is derived as

$$\begin{aligned}\langle\tilde{H}_0\rangle = \sum_k \Big[&\langle 0|\left[\chi^*(k)c_k + \chi^*(k+\pi)c_{k+\pi}\right]\left\{\epsilon(k)\left[c_k^\dagger c_k - c_{k+\pi}^\dagger c_{k+\pi}\right]\right. \\ &\left. + i\rho(k)\left[c_k^\dagger c_{k+\pi} - c_{k+\pi}^\dagger c_k\right]\right\}\left[\chi(k)c_k^\dagger + \chi(k+\pi)c_{k+\pi}^\dagger\right]|0\rangle\Big]\end{aligned} \tag{3.28}$$

again, applying Wicks theorem will give only four combinations which have non-zero values

$$\langle\tilde{H}_0\rangle = \sum_k \left[\epsilon(k)\left[|\chi(k)|^2 - |\chi(k+\pi)|^2\right] + i\rho(k)\left[\chi^*(k)\chi(k+\pi) - \chi^*(k+\pi)\chi(k)\right]\right] \tag{3.29}$$

To solve expectation values of $\tilde{H}_{int}$ we have to decouple k and k' momenta. We can use the Hartree-Fock decoupling [38] which, in second quantization formalism, is written as following

$$\begin{aligned}\langle\tilde{H}_{int}\rangle &= -\frac{V}{L}\sum_{k,k',q}\epsilon(q)\langle c_{k+q}^\dagger c_k c_{k'-q}^\dagger c_{k'}\rangle \\ &\approx -\frac{V}{L}\sum_{k,k',q}\epsilon(q)\left[\langle c_{k+q}^\dagger c_k\rangle\langle c_{k'-q}^\dagger c_{k'}\rangle - \langle c_{k+q}^\dagger c_{k'}\rangle\langle c_{k'-q}^\dagger c_k\rangle\right]\end{aligned} \tag{3.30}$$

the first term in above equation is known as Hartree decoupling while the second is called Fock decoupling. Hartree decoupling basically deals with interactions when two particles with momenta k and $k+q$ scatter from each other and come back to their original positions after scattering. Fock decoupling takes care of interactions when two particles exchange their positions after scattering. This behavior is depicted in Figure. 3.2. To find expectation values, all we need to do now is to choose the value of q such that k and k' are decoupled. Usually, only $q = 0$ terms give non-zero expectation values but as the system under study is at

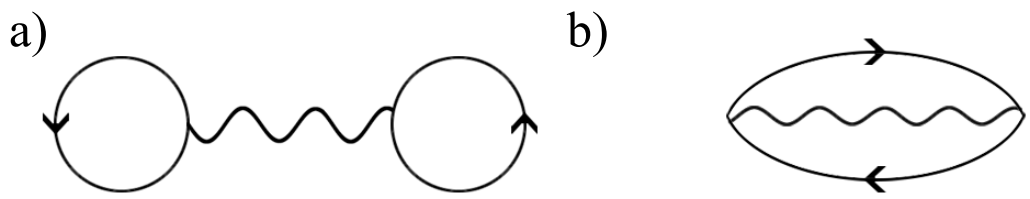

Figure 3.2: Feynman diagrams of Hartree and Fock interactions. *a*) Hartree decoupling: after interaction particle come back to its initial position. *b*) Fock decoupling: particles exchange positions with each-other after the interaction.

half-filling so Fermi wave vector is nested i.e. after $k = \pi$ Fermi surface repeats itself. It means that there are two types of non-zero expectation values one at $q = k' - k = 0$ and other is at $q = k' - k = \pi$. Usually, the first one is known as normal expectation values and the second is known as anomalous expectation values.

With $q = 0$ Hartree term (HT) gives

$$HT_{q=0} = -\frac{V}{L}\epsilon(0)\Big(\sum_k \langle c_k^\dagger c_k\rangle\Big)^2$$

as $c_k^\dagger c_k = n_k$ is density operator and summation over k makes it number of total particles in system which are $L/2$ so

$$HT_{q=0} = \frac{V}{L}\frac{L^2}{4} = \frac{VL}{4} \tag{3.31}$$

HT with $q = \pi$

$$\begin{aligned} HT_{q=\pi} &= -\frac{V}{L}\epsilon(\pi)\Big(\big[\sum_k \langle c_{k+\pi}^\dagger c_k\rangle\big]\big[\sum_{k'} \langle c_{k'-\pi}^\dagger c_{k'}\rangle\big]\Big) \\ &= -\frac{V}{L}\Big(\big[\sum_k \langle c_{k+\pi}^\dagger c_k\rangle\big]\big[\sum_{k'} \langle c_{k'}^\dagger c_{k'+\pi}\rangle\big]\Big) \\ &= -\frac{V}{L}\Big|\sum_k \langle c_{k+\pi}^\dagger c_k\rangle\Big|^2 \end{aligned} \tag{3.32}$$

where we have put $k = k + \pi$ in second step. Following the same procedure that we followed for deriving expectation values of $\tilde{H}_0$ we can evaluate (3.32) as

$$HT_{q=\pi} = -\frac{V}{L}\Big|\sum_k \chi^*(k+\pi)\chi(k)\Big|^2 \tag{3.33}$$

With $q = k' - k$, Fock term (FT) is

$$FT_{q=0} = \frac{V}{L}\Big(\sum_{k,k'} \epsilon(k'-k)\langle c^\dagger_{k+k'-k} c_{k'}\rangle \langle c^\dagger_{k'-k'-k} c_k\rangle\Big)$$

$$= \frac{V}{L}\Big(\sum_{k,k'} \epsilon(k'-k)\langle c^\dagger_{k'} c_{k'}\rangle \langle c^\dagger_k c_k\rangle\Big) = -\frac{V}{L}\Big(\sum_k \epsilon(k)\langle c^\dagger_k c_k\rangle\Big)^2$$

$$FT_{q=0} = -\frac{V}{L}\Big(\sum_k \epsilon(k)|\chi(k)|^2\Big)^2 \tag{3.34}$$

Similarly, FT with $q = \pi$ give

$$FT_{q=\pi} = \frac{V}{L}\Big(\sum_{k,k'} \epsilon(k'-k+\pi)\langle c^\dagger_{k+k'-k+\pi} c_{k'}\rangle \langle c^\dagger_{k'-k'+k-\pi} c_k\rangle\Big)$$

$$FT_{q=\pi} = -\frac{V}{L}\Big|\sum_k \epsilon(k)\chi^*(k+\pi)\chi(k)\Big|^2 \tag{3.35}$$

Putting results of Eq. (3.31), (3.33), (3.34) and (3.35) in (3.30) we get total interaction energy as following

$$\langle H_{int}\rangle = \frac{VL}{4} - \frac{V}{L}\Big[\Big|\sum_k \chi^*(k+\pi)\chi(k)\Big|^2 + \Big(\sum_k \epsilon(k)|\chi(k)|^2\Big)^2$$

$$+ \Big|\sum_k \epsilon(k)\chi^*(k+\pi)\chi(k)\Big|^2\Big] \tag{3.36}$$

Solving these terms numerically in this form takes a lot of time and it's not possible to take the derivative of absolute terms numerically. So, we have to simplify them. For purpose of simplicity let's solve $|\chi(k)|^2, |\chi(k+\pi)|^2, \chi^*(k)\chi(k+\pi)$ and $\chi^*(k+\pi)\chi(k)$ separately

$$|\chi(k)|^2 = \chi^*(k)\chi(k)$$

$$= \frac{1}{2\cosh[2\alpha h(k)]}\Big[\cosh[\alpha h(k)] - \epsilon(k)\frac{\sinh[\alpha h(k)]}{h(k)} - i\rho(k)\frac{\sinh[\alpha h(k)]}{h(k)}\Big]$$

$$\Big[\cosh[\alpha h(k)] - \epsilon(k)\frac{\sinh[\alpha h(k)]}{h(k)} + i\rho(k)\frac{\sinh[\alpha h(k)]}{h(k)}\Big]$$

$$= \frac{1}{2} - \frac{\epsilon(k)}{2h(k)}\tanh[2\alpha h(k)] \tag{3.37}$$

where $\epsilon^2(k) + \rho^2(k) = h^2(k)$. Similarly, $|\chi(k+\pi)|^2$ can also be calculated as

$$|\chi(k+\pi)|^2 = \chi^*(k+\pi)\chi(k+\pi)$$

$$= \frac{1}{2} + \frac{\epsilon(k)}{h(k)}\sinh[2\alpha h(k)] \tag{3.38}$$

where we used $h(k+\pi) = h(k)$. $\chi^*(k)\chi(k+\pi)$ and $\chi^*(k+\pi)\chi(k)$ are

$$\chi^*(k)\chi(k+\pi) = \frac{1}{2\cosh[2\alpha h(k)]} - \frac{i\rho(k)}{2h(k)}\tanh[2\alpha h(k)] \tag{3.39}$$

$$\chi^*(k+\pi)\chi(k) = \frac{1}{2\cosh[2\alpha h(k)]} + \frac{i\rho(k)}{2h(k)}\tanh[2\alpha h(k)] \tag{3.40}$$

Putting (3.37), (3.38), (3.39) and (3.40) in (3.29) we will get the final form of expectation value of $\tilde{H}_0$ as

$$\begin{aligned}\langle\tilde{H}_0\rangle &= \sum_k \left[-\frac{\epsilon^2(k)}{h(k)}\tanh[2\alpha h(k)] + \frac{i^2\rho^2(k)}{h(k)}\tanh[2\alpha h(k)]\right] \\ \langle\tilde{H}_0\rangle &= -\sum_k h(k)\tanh[2\alpha h(k)]\end{aligned} \tag{3.41}$$

Similarly, (3.36) will become

$$\begin{aligned}\langle\tilde{H}_{int}\rangle = \frac{VL}{4} - \frac{V}{L}\Bigg[&\left| \sum_k \frac{1}{2\cosh[2\alpha h(k)]} + \frac{i\rho(k)}{2h(k)}\tanh[2\alpha h(k)]\right|^2 \\ &+ \left(\frac{\epsilon(k)}{2} - \frac{\epsilon^2(k)}{2h(k)}\tanh[2\alpha h(k)]\right)^2 + \left| \sum_k \frac{\epsilon(k)}{2\cosh[2\alpha h(k)]}\right. \\ &\left. + \frac{i\epsilon(k)\rho(k)}{2h(k)}\tanh[2\alpha h(k)]\right|^2\Bigg]\end{aligned} \tag{3.42}$$

Total ground-state energy is sum of (3.41) and (3.42) while α is chosen such that energy is minimum. If we put $\delta = 0$ in the above derived expressions for energy, we can retrieve energy expressions for the Hubbard model which were calculated in Ref.[35].

3.5 Parent Hamiltonian of Baeriswyl wave function

A two-state effective parent Hamiltonian in k-space can be a great help to visualize phase transition and to check if the derived wave function is correct or not. This is done by plotting the curves traced out by $\mathbf{h(k)}$ vector when k is swiped

through the Brillouin zone. To construct parent Hamiltonian of BWF, consider that the Hamiltonian is given as

$$H_P = \xi(k) \begin{bmatrix} \cos\theta_k & \sin\theta_k e^{i\phi_k} \\ \sin\theta_k e^{-i\phi_k} & -\cos\theta_k \end{bmatrix} \tag{3.43}$$

and its ground-state wave function η is

$$|\eta\rangle = \begin{bmatrix} \sin\frac{\theta_k}{2} e^{i\phi_k} e^{i\beta} \\ -\cos\frac{\theta_k}{2} e^{i\beta} \end{bmatrix} \tag{3.44}$$

where β is some arbitrary phase. To completely define H_P we need to evaluate θ_k, ϕ_k and $\xi(k)$. Comparing (3.45) with (3.26)

$$\chi(k) = \sin\frac{\theta_k}{2} e^{i\phi_k} e^{i\beta}; \qquad \chi(k) = -\cos\frac{\theta_k}{2} e^{i\beta} \tag{3.45}$$

We can solve these equations for θ_k and ϕ_k

$$\phi_k = \tan^{-1}\left(\frac{\Im(Q)}{\Re(Q)}\right); \qquad \theta_k = 2\tan^{-1}\left(\frac{-\Re(Q)}{\cos\phi}\right) \tag{3.46}$$

where $Q = \chi(k)/\chi(k+\pi)$ and $\chi(i)$ is given by (3.26). To find $\xi(k)$ one can assume that total energy E is equal to $\sum_k \xi(k)$. Here total energy is sum of (3.41) and (3.42) except for the constant $VL/4$ i.e.

$$E = \sum_k \xi(k) = -\sum_k h(k)\tanh[2\alpha h(k)] - \frac{V}{L}\sum_{i=1}^{3} \left|\sum f_i(k)\right|^2 \tag{3.47}$$

where f_1 is given by (3.40), f_2 is $\epsilon(k)$ times (3.37) and f_3 is $\epsilon(k)$ times (3.40). The above equation gives $\xi(k)$

$$\xi(k) = -h(k)\tanh[2\alpha h(k)] - \frac{V}{L}\sum_{i=1}^{3}[f_i^*(k)\sum_k f_i(k)] \tag{3.48}$$

Sum of $\xi(k)$ over all k points in Brillouin zone is equal to total energy E.

Chapter 4

Polarization and Cumulants of the Zak phase

In this chapter, we will calculate the cumulants of polarization probability distribution for interacting SSH model and reconstruct the distribution. For this purpose, we will discuss the modern theory of polarization which is based on the Zak phase (a type of geometrical phases).

4.1 Geometric phase in quantum mechanics

In classical and quantum physics, the geometrical phase is the phase difference acquired by the system when it adiabatically makes a cycle in the parametric space. Shown in Figure. 4.1, a set of vectors is being parallelly transported on the surface of the sphere in a closed path. At the end of the path, vectors have acquired an extra phase of $\pi/2$ degrees, this extra phase is known as the geometrical phase. It was first generalized by M. V. Berry in 1984, hence it's also known as Berry phase[16]. Geometrical phase plays a very crucial rule in the understanding of many quantum phenomena e.g. Aharonov-Bohm (AB) effect, spin-orbit coupling and quantum Hall effect. A classical example of a geometrical

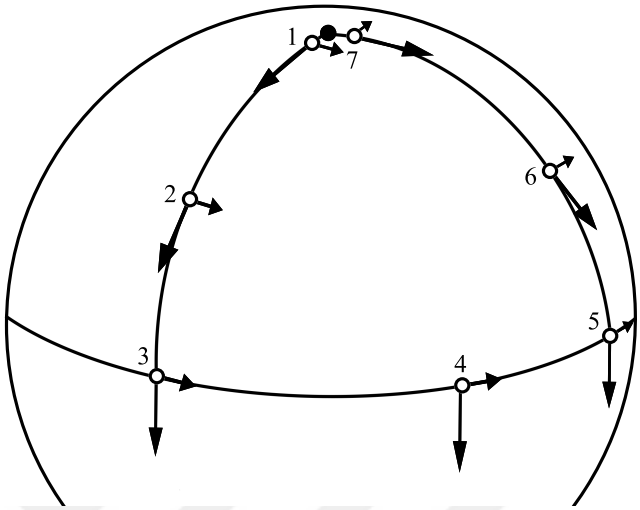

Figure 4.1: Schematic of geometrical phase. Vectors starting from solid black point, when parallel transported in a cycle, acquired an extra phase of $\pi/2$ due to the geometry of the sphere.

phase is Foucault pendulum which seems to change the plane of rotation, by a very small angle, every day due to rotation of the earth.

In quantum mechanics, this phase was first calculated by Zak for 1D solids. So, Berry phase in solids is known as the Zak phase. Electrons are in energy bands and when an external electrical field is applied, they begin to move. When electrons make a complete cycle, they acquire an extra phase, known as Zak phase. Berry phase has three properties:

1. It's purely geometric
2. It's always real
3. A phase factor is associated with all the paths that can be taken

Consider a half-spin in the magnetic field which is depending on time. Its Hamiltonian can be written as

$$\mathbf{H} = -\vec{\mathbf{B}}(t) \cdot \vec{\mathbf{S}} \tag{4.1}$$

suppose ground-state is $|n(t)\rangle$ such that $\mathbf{H}|n(t)\rangle = E_0|n(t)\rangle$ and $\vec{\mathbf{S}}.\hat{n}|n(t)\rangle = \hbar/2|n(t)\rangle$. We want to evolve system in time. First suppose that $\vec{\mathbf{B}} = B\hat{n}$ is not

changing with time and we evolve system in time from $t = 0$ to $t = \tau$. If $B\hat{n}$ is constant then at $t = 0$ ground state is $|n(0)\rangle$ and at some time $t = \tau$ ground state is $|n(\tau)\rangle = |n(0)\rangle$. Evolving system gives

$$\begin{aligned}\langle n(\tau)| \exp\left[\frac{-i}{\hbar}\int_0^T H dt\right]|n(0)\rangle &= \langle n(0)| \exp\left[\frac{-i}{\hbar}HT\right]|n(0)\rangle \\ &= \exp(\frac{-i}{\hbar}E_0 T) \end{aligned} \tag{4.2}$$

which is a very well known dynamical phase shift. Now, if we take adiabatically changing $\mathbf{B}$ such that $\mathbf{B} = B \cdot \hat{n}(t)$ and assume that this change is so slow that ground-state does not change and again we evolve system from $t = 0$ to $t = \tau$

$$\langle n(\tau)| \exp\left[\frac{-i}{\hbar}\int_0^T \mathbf{H} dt\right]|n(0)\rangle = \langle n(\tau)| \exp\left[\frac{i}{\hbar}\int_0^T -\vec{\mathbf{B}} \cdot \vec{\mathbf{S}} dt\right]|n(0)\rangle$$

by dividing total time T into N small intervals of Δt, it is easy to show that

$$\langle n(\tau)| \exp\left[\frac{-i}{\hbar}\int_0^T \mathbf{H} dt\right]|n(0)\rangle = \exp(\frac{-i}{\hbar}E_0 T) \exp(i\phi_B)$$

with

$$\phi_B = i \int dt \langle n(t)|\partial_t|n(t)\rangle \tag{4.3}$$

This extra phase ϕ_B is known as Berry phase. In this example we evolved system w.r.t time, in general one can take any parameter in which system can be evolved. In solids, electrons are evolved in momentum vector k. So, Berry phase in solids (also known as Zak phase) is written as

$$\phi_{zak} = i \int dk \langle n(k)|\partial_k|n(k)\rangle \tag{4.4}$$

Obviously, ϕ_{zak} is gauge dependent. By transforming

$$|n(k)\rangle \rightarrow e^{i\chi(k)}|n(k)\rangle$$

ϕ_{zak} become

$$\begin{aligned}\tilde{\phi}_{zak} &= i \int dk \Big[\langle n(k)|\partial_k|n(k)\rangle + i\partial_k \chi(k)\Big] \\ &= \phi_{zak} - \int dk \partial_k \chi(k) = \phi_{zak} - \chi(k(T)) + \chi(k(0)) \end{aligned} \tag{4.5}$$

So, Zak phase is gauge dependent but if we take a cyclic evolution of the system such that $\chi(k(T)) = \chi(k(0))$ then Zak phase can be considered as gauge independent, in other words

$$\chi(k(0)) - \chi(k(T)) = 2\pi(integer) \tag{4.6}$$

Therefore, we can say that the Zak phase can change only by multiple of 2π under gauge transformation but it can never be eliminated. And on a closed path, it's gauge independent.

4.1.1 Wannier functions and Zak phase

To describe bulk properties of crystalline solids we take non-interacting approximation in which sum of one-particle Hamiltonians makes the Hamiltonian of the complete system i.e.

$$H = \sum_{i=1}^{N} \left(\frac{p_i^2}{2m} + U(\mathbf{r}_i) \right) \tag{4.7}$$

where first term is kinetic energy and second is potential of $i-th$ particle. N is total number of particles and $U(\mathbf{r})$ is periodic under $\mathbf{R_n}$ lattice vector i.e. $U(\mathbf{r_i} + \mathbf{R_n}) = U(\mathbf{r_i})$. Solution of N particles can be obtained by solving Schrödinger equation

$$H_i\psi_i(\mathbf{r}) = E_i\psi_i(\mathbf{r}) \tag{4.8}$$

Where $H_i, \psi_i(\mathbf{r})$ and E_i are Hamiltonian, eigenstate and eigenvalue of $i-th$ particle. Because bulk is translational invariant so ground state of Hamiltonian is given by Bloch theorem

$$\psi_{\mathbf{k}}(\mathbf{r} + \mathbf{R_n}) = e^{i\mathbf{k}\cdot\mathbf{R_n}}\psi_{\mathbf{k}}(\mathbf{r}) \tag{4.9}$$

where $\mathbf{k}$ is the wave vector which is taken as discrete points in the Brillouin zone. Above equation can also be written as

$$\psi_{\mathbf{k}}(\mathbf{r}) = e^{ik\cdot\mathbf{r}}u_{\mathbf{k}}(\mathbf{r}) \tag{4.10}$$

where $u_{\mathbf{k}}(\mathbf{r})$ has the periodicity of lattice. Using (4.10), (4.8) can be written as

$$\left[\frac{(p + \hbar\mathbf{k})^2}{2m} + U(\mathbf{r}) \right] u_{n,\mathbf{k}}(\mathbf{r}) = E_{n,\mathbf{k}}u_{n,\mathbf{k}}(\mathbf{r}) \tag{4.11}$$

Bloch functions are a fully delocalized basis. They are periodic under reciprocal space vector **G** and their Fourier transformation gives localized Wanniar functions $W_n(j)$. In 1D

$$W_n(j) = \frac{1}{\sqrt{N}} \sum_k e^{-ijk} \psi_n(k) \tag{4.12}$$

Wannier functions obey following orthonormality relation

$$\int W_n^*(j) W_{n'}(j) = \delta_{n,n'} \tag{4.13}$$

Center of $j-th$ Wannier function, $r_n(j)$ is defined by

$$r_n(j) = \langle W_n(j) | \hat{r} | W_n(j) \rangle \tag{4.14}$$

where $\hat{r}$ is position operator. Bloch functions $|\psi_n(k)\rangle$ are decomposed as

$$|\psi_n(k)\rangle = |k\rangle \otimes |u_n(k)\rangle \tag{4.15}$$

for SSH model $n = 1, 2$ is conduction and valance bands respectively and $|u_n(k)\rangle$ are eigenstates. $|k\rangle$ can be Fourier transformed as

$$|k\rangle = \frac{1}{\sqrt{N}} \sum_{l=1}^{N} e^{ikl} |l\rangle \tag{4.16}$$

by applying $\hat{r}$ on $|W_n(j)\rangle$ we get

$$\begin{aligned}
\hat{r}|W_n(j)\rangle &= \hat{r} \frac{1}{N} \sum_k e^{-ijk} \sum_l e^{ilk} |l\rangle \otimes |u_n(k)\rangle \\
&= \frac{1}{N} \sum_k e^{-ijk} \sum_m m e^{imk} |m\rangle \otimes |u_n(k)\rangle \\
&= \frac{1}{2\pi} \int_0^{2\pi} dk e^{-ijk} \sum_m m e^{imk} |m\rangle \otimes |u_n(k)\rangle \\
&= \frac{-i}{2\pi} \int_0^{2\pi} dk \partial_k \sum_m e^{i(m-j)k} |m\rangle \otimes |u_n(k)\rangle + j \Bigg[\frac{1}{2\pi} \int_0^{2\pi} dk \sum_m e^{i(m-j)k} \\
&|m\rangle \otimes |u_n(k)\rangle \Bigg] + \frac{i}{2\pi} \int_0^{2\pi} dk \sum_m e^{i(m-j)k} |m\rangle \otimes \partial_k |u_n(k)\rangle
\end{aligned} \tag{4.17}$$

where in third step we have taken the thermodynamic limit $N \to \infty \Rightarrow k \to$ continuous. The first term in above equation is zero because of the periodicity

and the term in the bracket is a definition of Wannier function

$$\hat{r}|W_n(j)\rangle = j|W_n(j)\rangle + i\frac{1}{2\pi}\int_0^{2\pi} dk \sum_m |m\rangle \otimes \partial_k |u_n(k)\rangle$$

$$\langle W_n(j)|\hat{r}|W_n(j)\rangle = j + \frac{i}{2\pi}\int \langle u_n(k)|\partial_k|u_n(k)\rangle \tag{4.18}$$

Using (4.4)

$$r_n(j) = j + \frac{\phi_{zak}}{2\pi} \tag{4.19}$$

This equation gives the center of $j-th$ Wannier function in $n-th$ band and shows that all the centers of Wannier functions are equally spaced. We have successfully connected ϕ_{zak} with Wannier functions, now we can derive a relation between the polarization of material and Wannier functions.

4.2 Polarization in terms of the Zak phase

The most advanced theory of polarization before the modern theory of polarization was Clasusius-Mossoti (CM) theory [39]. The main idea of CM was to schematize the solid as the arrangement of separated and independent units, as shown in Figure. 4.2. But this kind of charge distribution only found in extreme ionic materials. In covalent materials, charge is so much delocalized that it's not possible to define a well separated and independent unit cell. Keeping in mind that macroscopic polarization is defined as "electric dipole moment per unit volume", there are few methods to define polarization in classical mechanics i.e.

1.
$$\mathbf{P}_{samp} = \frac{1}{V_{samp}}\int_{samp} d\mathbf{r}\mathbf{r}\rho(\mathbf{r}) \tag{4.20}$$

2.
$$\mathbf{P}_{cell} = \frac{1}{V_{cell}}\int_{cell} d\mathbf{r}\mathbf{r}\rho(\mathbf{r}) = \frac{1}{V_{cell}}\sum_i q_i\mathbf{r_i} \tag{4.21}$$

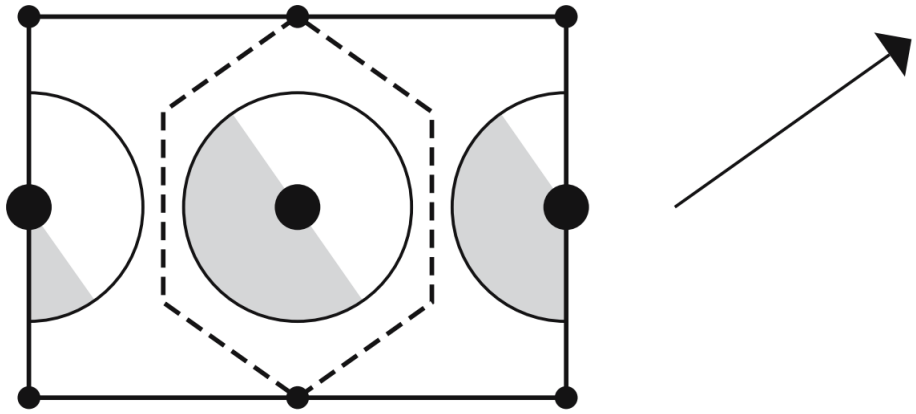

Figure 4.2: Polarized NaCl ionic crystal structure, represented within Clausius-Mossoti theory. Small circles are cations and big circles are anions. The shaded region is the electronic charge distribution and dashed line shows the boundary of the unit cell. The arrow at the right is showing the direction of polarization.

3.

$$\nabla \cdot \mathbf{P}_{micro}(r) = -\rho(\mathbf{r}) \tag{4.22}$$

Where $\rho(\mathbf{r})$ is volume charge density, V is volume, q is charge and $\mathbf{r_i}$ is position of $i-th$ charge. We will see that all these three methods fail to completely define bulk polarization. Polarization is only a bulk phenomenon but in the first method, the integral cannot distinguish between surface and bulk contributions of charge. For example, if we have a cube of dimension $L \times L \times L$ and prepared such that charge on left surface is $+\sigma$ and on right is $-\sigma$. This will change the charge density and hence polarization of system, even though there were no changes in the bulk of the material. Thus, the first way of defining bulk polarization is not a good definition. To see shortcomings of the second definition, we will discuss an example. Suppose we have a 1D chain of alternating charged particles as shown in Figure. 4.3. There are two choices of a unit cell. Consider left edge of unit cell is at $x = 0$ and charge of anion(cation) is $-1(+1)$. Polarization in the left unit cell is

$$P_{left} = \sum_i q_i x_i = \frac{1}{a}\left(\frac{-a}{4} + \frac{3a}{4}\right) = \frac{1}{2} \tag{4.23}$$

By using the same steps, we can calculate that the polarization of right unit cell is $-1/2$ which is in contradiction with the polarization of left unit cell.

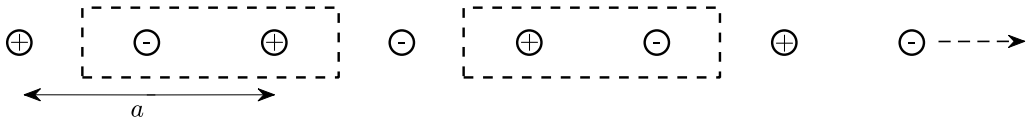

Figure 4.3: 1D chain of alternating charged particles with the distance between two anions a. The dashed rectangular indicate unit cells.

There are many other ways to define a unit cell which can give polarizations $\cdots -5/2, -3/2, -1/2, 1/2, 3/2, 5/2 \cdots$. Notice that polarization is changing by a unit. This unit is called quanta of polarization. Hence, the second definition of polarization is not a unique way to define polarization. The third definition of polarization is also not unique as one can add any term with zero divergence i.e. $\nabla \cdot P = \nabla \cdot (P + C)$ where C is any constant.

4.2.1 Polarization as an adiabatic flow of current

As all classical ways to define polarization have failed, we need to build a new definition of polarization by taking quantum aspects into account. Before that, we should note that experimentally we actually do not need the absolute value of polarization but the change in polarization. For example, pyroelectric coefficient

$$\Pi_\alpha = \frac{dP_\alpha}{dT} \tag{4.24}$$

defined as derivative with respect to temperature T, permittivity

$$\chi_{\alpha\beta} = \frac{dP_\alpha}{d\varepsilon_\beta} \tag{4.25}$$

defined as derivative with respect to field, ε_β and piezoelectric tensor

$$\gamma_{\alpha\beta\delta} = \frac{\partial P_\alpha}{\partial \epsilon_{\beta\delta}} \tag{4.26}$$

defined as derivative with respect to strain, $\epsilon_{\beta\delta}$[40].
To build the theory which can calculate the change in polarization, we can start by taking an example of piezoelectricity, in which systems have a non-zero value of polarization when external strain is applied, Figure. 4.4. Suppose in unstrained

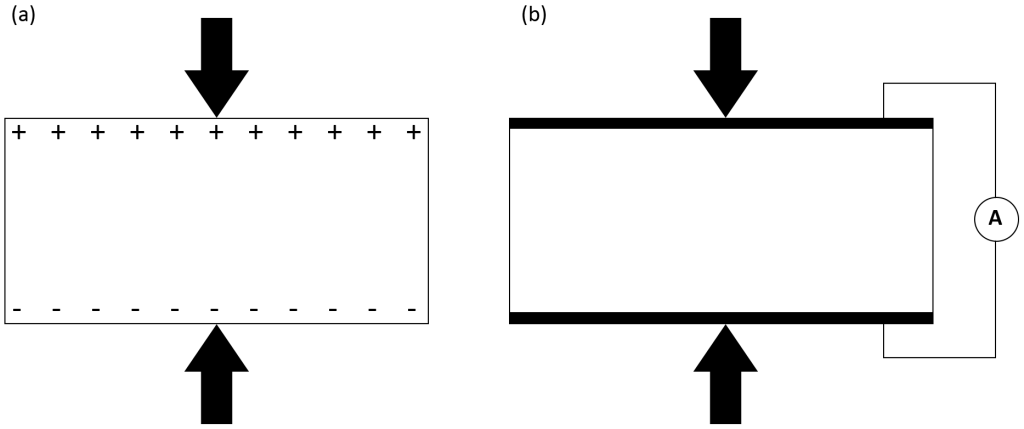

Figure 4.4: Piezoelectric effect in a system on which strain is applied along the piezoelectric axis. (a) The charge is induced on the surface of the crystal due to strain and (4.20) can be used to calculate polarization but surface charges cannot be distinguished in integral. (b) An external capacitor is used to short the circuit and polarization can be calculated using charge flow.

system polarization was zero and when strain is applied charge build on the sides of the system, a situation in (a), on which (4.20) can be used to calculate polarization but this way of calculation cannot untangle surface and bulk contribution to the integral. In (b), the situation of the modern theory of polarization is depicted and showing that piezoelectricity is only a bulk effect [40]. While the strain is applied, an electric charge flows through the system and can be measured carefully. Now, the polarization is not only calculated in the final state. In fact, the time dependence of (b) is a very essential feature, no matter how slow it is. Fundamental relation from electrodynamics is "change in polarization $\mathbf{P}$ is equal to current density $\mathbf{j}(t)$ flowing through the system" i.e.

$$\frac{d\mathbf{P}}{dt} = \mathbf{j}(t) \tag{4.27}$$

If the change is adiabatic, (4.27) can be solved for change is polarization

$$\int_0^{\Delta t} \frac{d\mathbf{P}}{dt} dt = \int_0^{\Delta t} \mathbf{j}(t) dt$$

$$\Delta\mathbf{P} = \mathbf{P}(\Delta t) - \mathbf{P}(0) = \int_0^{\Delta t} \mathbf{j}(t) dt \tag{4.28}$$

One can see that even for a perfectly adiabatically change (Δt goes to infinity and $\mathbf{j}(t)$ goes to zero) above integral remains finite. It is worth to note that measuring charge flow is much easier than dipole measurement, hence the situation given in Figure. 4.4 (b) is a more efficient way to represent actual polarization than (a). Similarly, ferroelectric polarization can be easily represented using the adiabatic flow of currents [40]. Therefore, we conclude that induced macroscopic polarization can be understood in term of adiabatic charge flow in the system. So, the basic concept of modern theory of polarization is (4.28). We can change adiabatic time to general dimensionless parameter λ where λ can change between 0 (initial system) and 1 (final system).

$$\Delta\mathbf{P} = \int_0^1 d\lambda \frac{d\mathbf{P}}{d\lambda} \tag{4.29}$$

Generally, the initial (final) system means the state of the system before (after) application of some adiabatic change.

4.2.2 Zak phase theory of polarization

In this subsection, there will be a discussion of continues and discrete formalism that connects polarization with the Zak phase.

4.2.2.1 Continuous Fourier-space formalism

Consider a many-body crystalline system with periodic boundary conditions and vanishing electric field for all value of λ. The eigenstate of such system is a Bloch state $|\psi_{nk}\rangle$ and obey Schrödinger equation i.e.

$$H|\psi_{n\mathbf{k}}\rangle = E_{n\mathbf{k}}|\psi_{n\mathbf{k}}\rangle; \qquad H = \frac{p^2}{2m} + V \tag{4.30}$$

where $E_{n\mathbf{k}}$ is eigenvalue, p is momentum and V is potential. Equivalently, above equation can be written as

$$H_k|u_{n\mathbf{k}}\rangle = E_{nk}|u_{n\mathbf{k}}\rangle; \qquad H_{\mathbf{k}} = \frac{(p+\hbar\mathbf{k})^2}{2m} + V \tag{4.31}$$

with u_{nk} has the periodicity of lattice. All terms given above depend upon parameter λ but for simplicity, we are suppressing λ in notations and will use it in the last expression. Using elementary perturbation theory, we can find current density [41, 42]

$$\mathbf{j}_n = \frac{ie\dot{\lambda}}{(2\pi)^3}\sum_{m\neq n}\int d\mathbf{k}\frac{\langle\psi_{n\mathbf{k}}|\partial_{\mathbf{k}}H|\psi_{m\mathbf{k}}\rangle\langle\psi_{m\mathbf{k}}|\partial_\lambda H|\psi_{n\mathbf{k}}\rangle}{(E_{n\mathbf{k}}-E_{m\mathbf{k}})^2} + c.c. \tag{4.32}$$

where $c.c.$ is complex conjugate, e is charge of electron, m is mass and $\dot{\lambda} = d\lambda/dt$. Note that $\partial_{\mathbf{k}}H = p/m$, $\partial_\lambda H = \partial_\lambda V$ and

$$\begin{aligned}\langle\psi_{n\mathbf{k}}|p|\psi_{m\mathbf{k}}\rangle &= \frac{m}{\hbar}\langle u_{n\mathbf{k}}|[\partial_{\mathbf{k}},H]|u_{m\mathbf{k}}\rangle \\ &= \frac{m}{\hbar}\big[E_{m\mathbf{k}}\langle u_{n\mathbf{k}}|\partial_{\mathbf{k}}|u_{m\mathbf{k}}\rangle - E_{n\mathbf{k}}\langle u_{n\mathbf{k}}|\partial_{\mathbf{k}}|u_{m\mathbf{k}}\rangle\big] \\ &= -\frac{m}{\hbar}(E_{n\mathbf{k}}-E_{m\mathbf{k}})\big[\langle u_{n\mathbf{k}}|\partial_{\mathbf{k}}|u_{m\mathbf{k}}\rangle\big]\end{aligned} \tag{4.33}$$

also

$$\begin{aligned}\langle\psi_{m\mathbf{k}}|\partial_\lambda V|\psi_{n\mathbf{k}}\rangle &= \langle u_{m\mathbf{k}}|[\partial_\lambda,H]|u_{n\mathbf{k}}\rangle \\ &= E_{n\mathbf{k}}\langle u_{m\mathbf{k}}|\partial_\lambda|u_{n\mathbf{k}}\rangle - E_{m\mathbf{k}}\langle u_{m\mathbf{k}}|\partial_\lambda|u_{n\mathbf{k}}\rangle \\ &= (E_{n\mathbf{k}}-E_{m\mathbf{k}})\big[\langle u_{n\mathbf{k}}|\partial_\lambda|u_{m\mathbf{k}}\rangle\big]\end{aligned} \tag{4.34}$$

using (4.33) and (4.34) in (4.32), we get

$$\mathbf{j}_n = \frac{-ie\dot{\lambda}}{(2\pi)^3}\sum_{m\neq n}\int d\mathbf{k}\langle u_{n\mathbf{k}}|\partial_{\mathbf{k}}|u_{m\mathbf{k}}\rangle\langle u_{m\mathbf{k}}|\partial_\lambda|u_{n\mathbf{k}}\rangle + c.c. \tag{4.35}$$

letting adiabatic parameter to be time i.e. $t\to\lambda$, $\dot{\lambda}=1$

$$\begin{aligned}\mathbf{j}_n = \frac{d\mathbf{P_n}}{dt} &= \frac{-ie}{(2\pi)^3}\sum_{m\neq n}\int d\mathbf{k}\langle u_{n\mathbf{k}}|\partial_{\mathbf{k}}|u_{m\mathbf{k}}\rangle\langle u_{m\mathbf{k}}|\partial_\lambda|u_{n\mathbf{k}}\rangle + c.c. \\ \frac{d\mathbf{P_n}}{dt} &= \frac{-ie}{(2\pi)^3}\int d\mathbf{k}\langle\partial_{\mathbf{k}}u_{n\mathbf{k}}|\partial_\lambda u_{n\mathbf{k}}\rangle + c.c.\end{aligned} \tag{4.36}$$

This is the contribution to the change of polarization due to $n-th$ particle. Total change in polarization can be summed up over N number of particles i.e.

$$\Delta\mathbf{P} = \int_0^1\frac{d\mathbf{P_n}}{d\lambda}d\lambda = \frac{-ie}{(2\pi)^3}\sum_{n=1}^{N}\int d\mathbf{k}\int_0^1 d\lambda\big[\langle\partial_{\mathbf{k}}u_{n\mathbf{k}}|\partial_\lambda u_{n\mathbf{k}}\rangle + c.c.\big] \tag{4.37}$$

Using partial integration, the above equation become

$$\Delta\mathbf{P} = \frac{-ie}{(2\pi)^3}\sum_{n=1}^{N}\int d\mathbf{k}\Big[-\int_0^1 d\lambda\partial_\lambda\langle u_{n\mathbf{k}}|\partial_{\mathbf{k}}|u_{n\mathbf{k}}\rangle - \int_0^1 d\lambda\partial_{\mathbf{k}}\langle u_{n\mathbf{k}}|\partial_\lambda|u_{n\mathbf{k}}\rangle\Big] \quad (4.38)$$

Last term will be zero because $u_{n\mathbf{k}}$ is periodic in k-space

$$\Delta\mathbf{P} = \frac{ie}{(2\pi)^3}\sum_{n=1}^{N}\int d\mathbf{k}\langle u_{n\mathbf{k}}|\partial_{\mathbf{k}}|u_{n\mathbf{k}}\rangle\Big|_0^1$$

$$\Delta\mathbf{P} = \mathbf{P}(1) - \mathbf{P}(0) \quad (4.39)$$

with

$$\mathbf{P}(\lambda) = \frac{ie}{(2\pi)^3}\sum_{n=1}^{N}\int d\mathbf{k}\langle u^{(\lambda)}_{n\mathbf{k}}|\partial_{\mathbf{k}}|u^{(\lambda)}_{n\mathbf{k}}\rangle \quad (4.40)$$

note we used notations for λ dependence of states that we had suppressed from the beginning. Using (4.4) we get final form of polarization

$$\mathbf{P} = \frac{e}{\mathbf{\Omega}}\sum_{n=1}^{N}\phi^n_{zak} \quad (4.41)$$

where $\mathbf{\Omega}$ is the volume of the unit cell and ϕ^n_{zak} is the Zak phase of $n-th$ band. Of course, this polarization is only for electrons in the systems, total polarization is the sum of electronic polarization and ionic polarization.

4.2.2.2 Formalism in discrete space

In computational calculation, we cannot use (4.41) as it is. We have to convert integral over k into discrete grid of $k-$ points. For purpose of simplicity, let's take case of 1D where $P_n = e\phi^n_{zak}/2\pi$ with ϕ_{zak} given by (4.4). Integral over k can be discretized as

$$\int dk\langle u_{nk}|\partial_k|u_{nk}\rangle \to \sum_{k_j} dk\langle u_{nk}|\partial_k u_{nk}\rangle\big|_{k=k_j} \quad (4.42)$$

As $u_{n,k+dk} \approx u_{nk} + \partial_k u_{nk}dk$, (Tylor series), so

$$\langle u_{n,k}|u_{n,k+dk}\rangle \approx 1 + \langle u_{n,k}|\partial_k u_{nk}\rangle dk$$

$$\ln[\langle u_{n,k}|u_{n,k+dk}\rangle] = \langle u_{nk}|\partial_k u_{nk}\rangle dk \quad (4.43)$$

putting (4.43) in (4.42)

$$\int dk \langle u_{n,k}|\partial_k|u_{n,k}\rangle \rightarrow \sum_{k_j} \ln\langle u_{n,k}|u_{n,k+dk}\rangle\big|_{k=k_j} \tag{4.44}$$

$k_j = 2\pi j/Na$, where N is total number of points on grid, $j = 0, 1, 2, \ldots N-1$, a is lattice constant and $dk = 2\pi/Na$. So, Zak phase of $n-th$ band become

$$\begin{aligned} \phi^n_{zak} &= -\Im \sum_j \ln\langle u_{nk_j}|u_{nk_{j+1}}\rangle \\ \phi^n_{zak} &= -\Im \prod_{j=0}^{N-1} \langle u_{n,k_j}|u_{n,k_{j+1}}\rangle \end{aligned} \tag{4.45}$$

4.2.2.3 Quanta of polarization

As polarization of one band is given by

$$\mathbf{P} = \frac{e}{\mathbf{\Omega}}\phi_{zak}$$

and ϕ_{zak} is only defined as the modulo of 2π, which translates that if we had chosen some other branch on which adiabatic change of system was taken then polarization could be

$$\begin{aligned} \tilde{\mathbf{P}} &= \frac{e}{\mathbf{\Omega}}[\phi_{zak} + 2\pi m] \\ \tilde{\mathbf{P}} &= \mathbf{P} + \frac{e\mathbf{R}}{\mathbf{\Omega}} \end{aligned} \tag{4.46}$$

where m is an integer and $\mathbf{R}$ is lattice vector. The last term in (4.46) is known as quantum of polarization.

Summing up everything so far, we have found the polarization given by (4.41) which is only well-defined modulo $e\mathbf{R}/\mathbf{\Omega}$. And the change in polarization during an adiabatic process is given by (4.29). Whole theory can be written as

$$\Delta\mathbf{P} := (\mathbf{P}(1) - \mathbf{P}(0)) \quad modulo \quad \frac{e\mathbf{R}}{\mathbf{\Omega}} \tag{4.47}$$

Actual mean of above equation is that $\Delta\mathbf{P}$ is equal to $\mathbf{P}(1) - \mathbf{P}(0) + e\mathbf{R}/\mathbf{\Omega}$ for any lattice vector $\mathbf{R}$.

4.3 Polarization probability distribution and cumulants

The cumulant function is the Laplace transformation of the probability distribution function and shows connectedness of n variables with each other. In statistics and probability theory, cumulants (C_n) of any distribution are alternative of moments from which complete distribution can be reconstructed. Moments and cumulants are related quantities, if one knows the expression for cumulants then moments can be calculated. Cumulants are defined by a cumulant generating function. The first cumulant gives information about the mean of the distribution, second gives variance. Third and fourth cumulant give information on asymmetric and kurtosis of distribution respectively.
As described in last section polarization is directly connected with the Zak phase. To calculate the probability distribution of polarization, we find cumulants associated with the Zak phase. And to calculate cumulants we start off by comparing product term of (4.45) with a cumulant generating function

$$\begin{aligned} \exp\left(\frac{1}{\Delta k}\sum_{n=1}^{\infty}\frac{(i\Delta k)^n}{n!}C_n\right) &= \prod_{j=0}^{N-1}\langle u_{n,k_j}|u_{n,k_{j+1}}\rangle \\ \frac{1}{\Delta k}\sum_{n=1}^{\infty}\frac{(i\Delta k)^n}{n!}C_n &= \ln\left[\prod_{j=0}^{N-1}\langle u_{n,k_j}|u_{n,k_{j+1}}\rangle\right] \\ &= \sum_{j}^{N-1}\ln\left[\langle u_{n,k_j}|u_{n,k_{j+1}}\rangle\right] \end{aligned} \tag{4.48}$$

note that

$$\begin{aligned} |u_{n,k_j+1}\rangle &= |u_{n,k}\rangle + \partial_k|u_{n,k}\rangle\Delta k + \partial_k^2|u_{n,k}\rangle\frac{\Delta k^2}{2!} + \dots \\ \langle u_{n,k}|u_{n,k_j+1}\rangle &= 1 + \gamma_1\Delta k + \gamma_2\frac{\Delta k^2}{2!} + \dots \end{aligned} \tag{4.49}$$

where $\gamma_i = \langle u_{n,k}|\partial_k^i|u_{n,k}\rangle$. Expanding ln into its series, using (4.49) in (4.48) and comparing like powers of Δk, we can find cumulants. First four cumulants are

given below

$$\tilde{C}_1 = -i \int dk \gamma_1 \tag{4.50a}$$

$$\tilde{C}_2 = - \int dk [\gamma_2 - \gamma_1^2] \tag{4.50b}$$

$$\tilde{C}_3 = i \int dk [\gamma_3 - 3\gamma_2\gamma_1 + 2\gamma_1^3] \tag{4.50c}$$

$$\tilde{C}_4 = \int dk [\gamma_4 - 3\gamma_2^2 - 4\gamma_3\gamma_1 + 12\gamma_1^2\gamma_3 - 6\gamma_1^4] \tag{4.50d}$$

where we have taken limit $\Delta k \to 0, N \to \infty$. Above given $\tilde{C}_i$ are gauge depended, as shown in 4.6. To make cumulants gauge independed, we can write them as

$$C_i = \frac{M}{2\pi} \tilde{C}_i \tag{4.51}$$

Where M is the number of sites in a unit cell. Simply, one can write γ_i for wave-function given in form $\prod_k (a x_k^\dagger + b y_k^\dagger)|0\rangle$ as $a^* \partial_k^i a + b^* \partial_k^i b$. If Wannier centers are spread in a way that they are only localized within one unit cell, then cumulants derived above can be taken as cumulants of Wannier centers [20]. The interacting SSH model we are studying is a lattice model i.e. the Wannier centers are totally localized on a specific site, this makes the above derived $C_i s$ cumulants of Wannier centers of SSH model.

Generating full probability distribution from only a few known cumulants is still a question in the study. However, there are many approximations and general distribution functions that can be used to approximate a distribution with only a few of its cumulants (or moments) known. One of the most reliable methods for reconstruction of distribution is maximum entropy method (MEM)[43, 44]. In MEM one maximizes the entropy of the system under constrained provided by the moments. There are some general distribution functions which can construct probability with only a few leading cumulants or moment. For example, general gamma and beta distribution functions can construct probability with first four cumulants. However, gamma distribution supports only $x = (0, \infty)$ and beta only support $x = [0, 1]$. This limitation makes both these distributions ill-suited for probability reconstruction of polarization for the SSH model because SSH model has "mean" on negative x (see chapter 5). There is Gaussian (normal) distribution which needs only the first two cumulants to reconstruction probability. One can

add skewness (third cumulant) to Gaussian distribution to get "skewed normal distribution". To construct full distribution, we have to know and use all of its cumulants or moments which is not possible. So, in this thesis, we used only first three cumulants to reconstruction probability distribution using a skewed normal distribution function. The skewed normal distribution function is defined as

$$P(x) = \frac{2}{\omega}\phi\left(\frac{x-\xi}{\omega}\right)\Phi\left(\alpha\left(\frac{x-\xi}{\omega}\right)\right) \tag{4.52}$$

with

$$\phi(i) = \frac{1}{\sqrt{2\pi}}e^{-\frac{i^2}{2}} \qquad \Phi(i) = \frac{1}{2}\left(1+\text{erf}(\frac{i}{\sqrt{2}})\right)$$

Note that here P is probability not polarization, x is random variable and erf is error function. α, ξ and ω are parameters of distribution. Mean (m), variance(v) and skewness(s) are given in terms of these parameters as

$$m = \xi + \omega\delta\sqrt{\frac{2}{\pi}} \tag{4.53a}$$

$$v = \omega^2\left(1 - \frac{2\delta^2}{\pi}\right) \tag{4.53b}$$

$$s = \frac{4-\pi}{2}\frac{(\delta\sqrt{2/\pi})^3}{(1-2\delta^2/\pi)^{3/2}} \tag{4.53c}$$

here $\delta = \frac{\alpha}{\sqrt{1+\alpha^2}}$. Note that here δ and α are not being used in context of SSH model. They are being used for a probability distribution function. One can find correct parameters (α, ξ and ω) by numerically solving above equations for chosen m, v and s.

Chapter 5

Results

BWF gives a very good approximation of ground-state energy for interacting SSH model. Comparison of BWF's total energy with ED calculations and minimization parameter is given in Figure. 5.1 for $\delta = 0, \pm 0.3, \pm 0.5$ and ± 0.7. This comparison gets little worse when δ is increased (decreased) from 0 to $1(-1)$. However, in extreme limits of V, value of energy is always exact. In limit $V \to \infty$, energy goes to zero because of large repulsion between particles. In limit $V \to 0$, energy is exactly equal to the energy of the non-interacting SSH model.

For all values of δ, there is a finite α that minimize the ground-state energy. But for each δ, there is a V_t on which this minimum become local minimum, with $\alpha = \infty$ as global minimum, see Figure. 5.2 and 5.3 for different δ and V. It means that in this variational approximation, there is a first order phase transition. For equal hopping between sites i.e. $\delta = 0$ (simple t-V model), there is a metal-insulator transition occurring at $V = 1.3365\ldots$, rather than $V = 2$ which is the result of exact solution. This is interesting because BWF is known for producing only insulating states but in this calculation a first-order transition is found. Note that only the GWF can produce metallic states but in our calculation we get this with BWF. The BWF was known to produce metallic states only in limit $\alpha \to \infty$ when projector $e^{-\alpha H_0}$ projects out all high kinetic energy states. But we find a metallic state at finite value of α

Phase diagram of interacting SSH is shown in Figure. 5.4(a). A and B are SSH

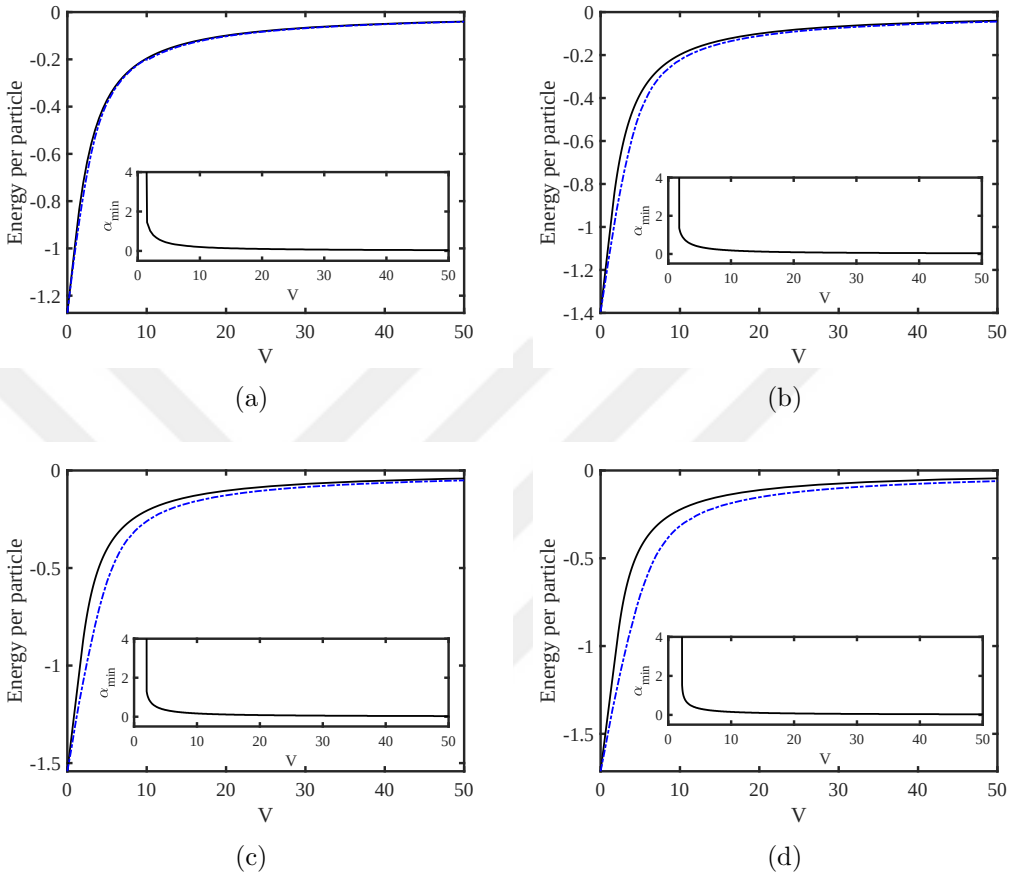

Figure 5.1: Comparison of energy per particle calculated by BWF (Black solid line) with ED calculations (Blue dashed-dotted line). Inset shows value of α that minimize the energy for chosen value of δ and V. In this calculation t is taken 1: (a) $\delta = 0$, (b) $\delta = \pm 0.3$, (c) $\delta = \pm 0.5$, (d) $\delta = \pm 0.7$

phases (Hartree-Fock approximation) and C is a CDW ordered insulating phase. When all hoping parameters are equal, there is a conducting phase (a Fermi sea in this calculation) for the small value of interaction (dotted-dashed line in phase diagram). And a correlated insulating phase with CDW ordering is found for the large value of interaction (Region C). For finite value of δ, with small interaction, there is an SSH ground-state (Region A and B) and when interaction is increased systems goes toward CDW state with non-zero skewness (third cumulant). Value of V at which phase transition occur is different for each δ, as shown in phase diagram.

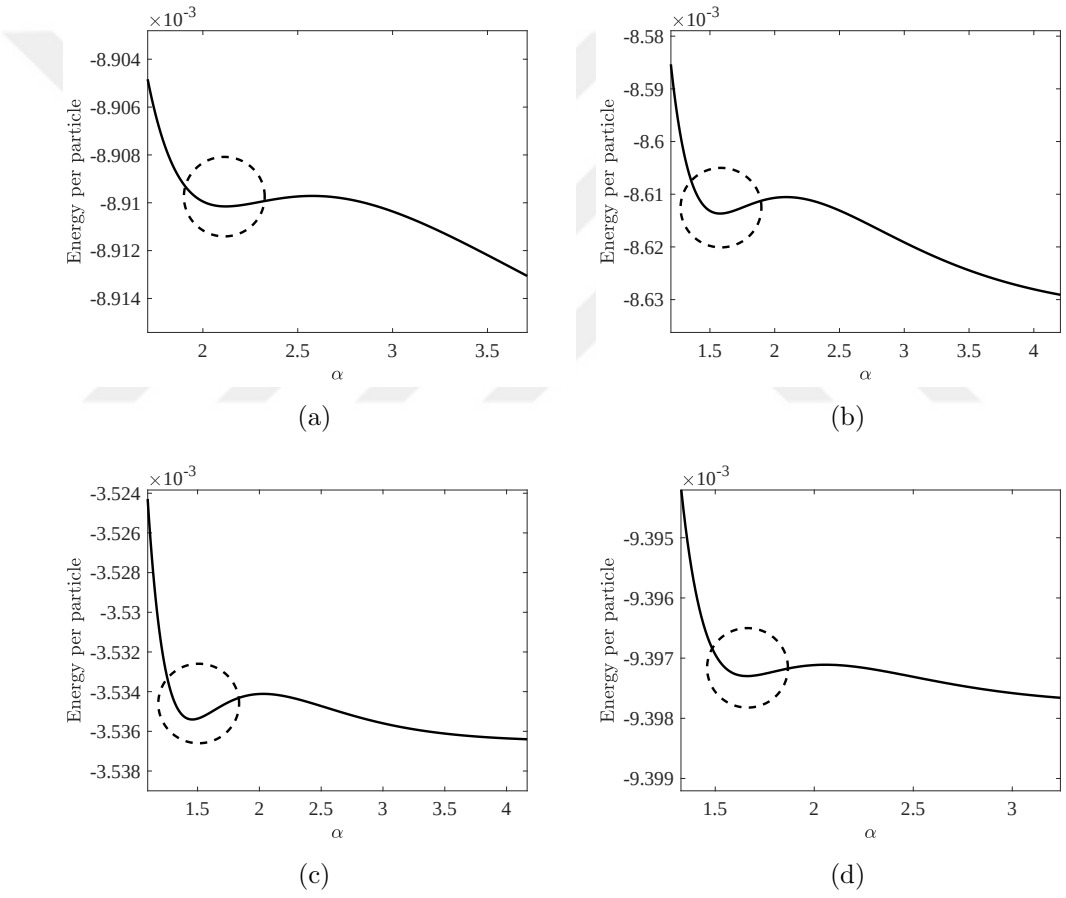

Figure 5.2: Presence of metastable states in system for: (a) $\delta = 0$ at $V = 1.280$, (b) $\delta = \pm 0.3$ at $V = 1.670$, (c) $\delta = \pm 0.5$ at $V = 1.950$, (d) $\delta = \pm 0.7$ at $V = 2.185$

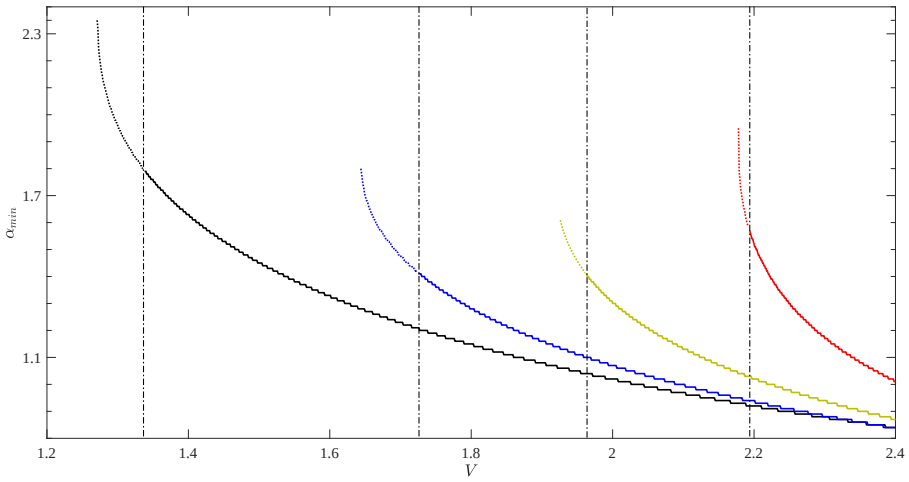

Figure 5.3: Values of V and respective α_{min} at which system is in metastable state (dotted line) and stable state (solid line). Black, blue, orange and red lines are for $\delta = 0, \pm 0.3, \pm 0.5$ and ± 0.7 respectively.

To begin with the analysis of polarization distribution, we first take $V = 0$ case (simple SSH model) and check if BWF produces correct cumulants. Comparison of cumulants calculated using exact wave function (2.12) with BWF (3.27) is shown in Figure. 5.4(b). It shows that BWF gives an excellent approximation of ground-state. First cumulant is $1/2(-1/2)$ for $\delta > 0 (\delta < 0)$. Second and fourth cumulants are finite for finite values of δ and at $\delta = 0$ all cumulants, except for the first which becomes zero, diverge to infinity. The third cumulant is zero for finite δ which shows that probability distribution is nearly a normal distribution (as in this thesis we used only first three cumulants for construction of probability distribution).

3D plots of the first four cumulants in parametric space of δ and V are given in Figures. 5.5. First cumulant (which is equal to first moment) varies between $1/2$ and $-1/2$. It shows that "mean" of probability is between these values. There is sharp discontinuity for $V < 1.3365\ldots$ which indicates the metallic behavior. It also suggests that non-trivial point ($\delta = 0$) of simple SSH model has become a line due to interaction. For a finite δ, the second cumulant decreases with increasing interaction which shows that increasing interaction makes probability distribution more localized around the mean. The third cumulant is zero for the

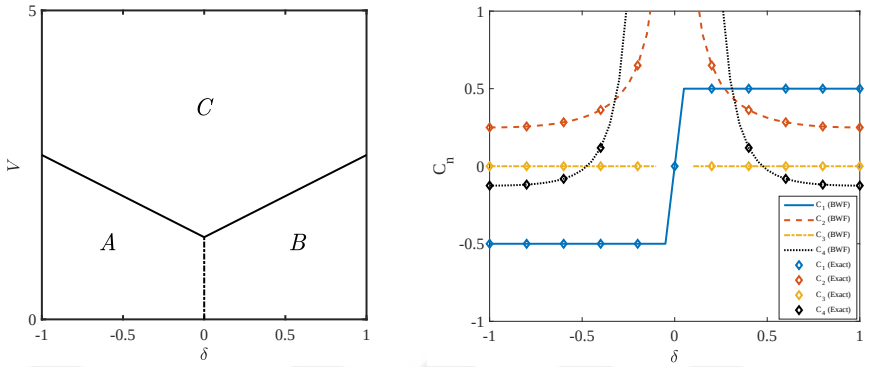

(a) (b)

Figure 5.4: (a) Phase diagram of interacting SSH model. A and B are SSH states and C is CDW ordering insulating state. Dotted-dashed line is a Fermi sea (metal), (b) Comparison of cumulants calculated by exact wave function with BWF at $V = 0$.

A and B phases and becomes positive (negative) for $\delta > 0 (\delta < 0)$ in C phase. It shows that the probability distribution is skewed toward the center of the cell. Cumulants for $\delta = 0, 0.3, 0.5$ and 0.7 are shown in Figure. 5.6. Respective probability distribution calculated by only the first three cumulants is given in Figure. 5.7. The same kind of relationship is found for other values of δs. It shows that for each δ when interaction increase, distribution become more localized around zero (center of the unit cell). It's because with increasing interaction, first and second cumulant move toward zero.

To study effect of interaction on distribution, we take two paths which connect two distinct topological phases separated by topological non-trivial line. Both paths are taken at non-zero value of V. Path-I is taken at constant $V = 1$ form $\delta = 1$ to $\delta = -1$. And path-II is taken from $\delta = 1$ and $V = 1$ to $\delta = -1$ and $V = 1$ making an eclipse in parameter space of δ and V, as shown in Figure. 5.8(a). This eclipse follows equation $\delta = \cos(\phi), V = 1 + 4\sin(\phi)$ and ϕ is taken between 0 and π. Cumulants calculated on both paths are given in Figure. 5.8(b) and 5.8(c) respectively. The probability distribution constructed on both paths is shown in Figure. 5.9.

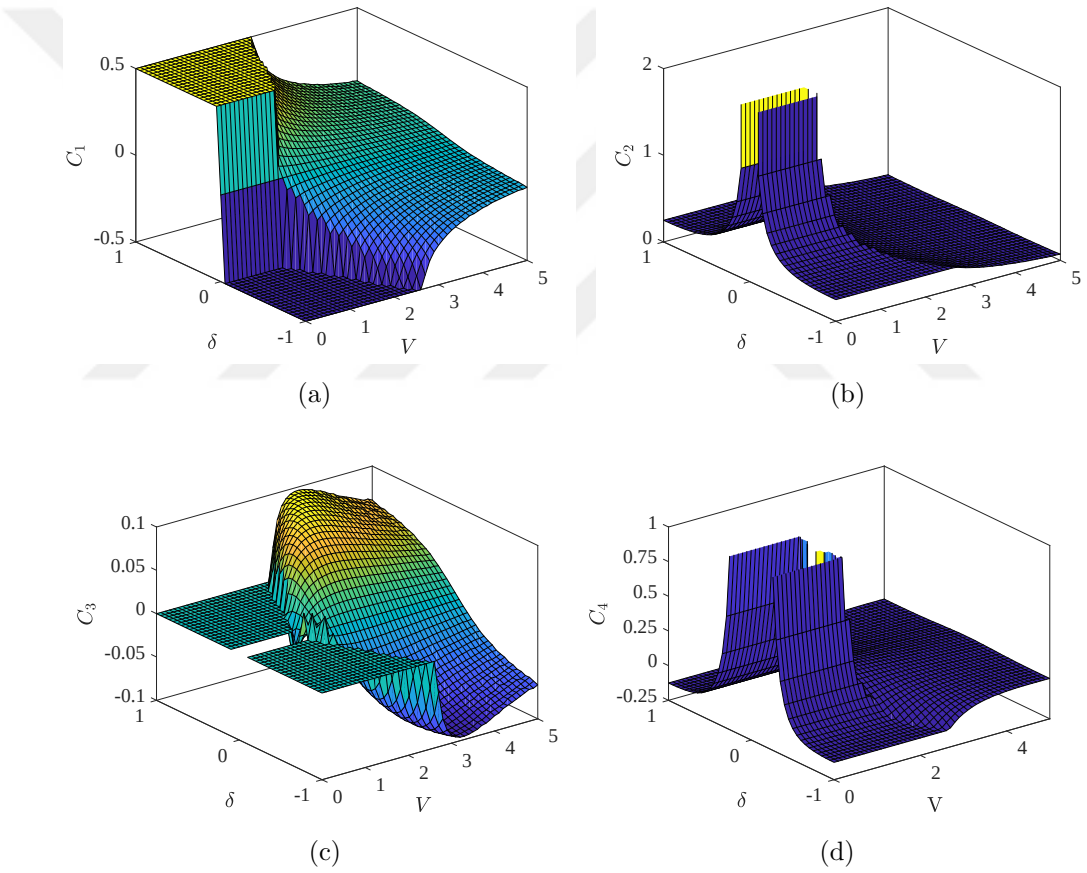

Figure 5.5: 3D plots of four cumulants and moments. (a) First cumulant, (b) Second cumulant, (c) Third cumulant, (d) Fourth cumulant,

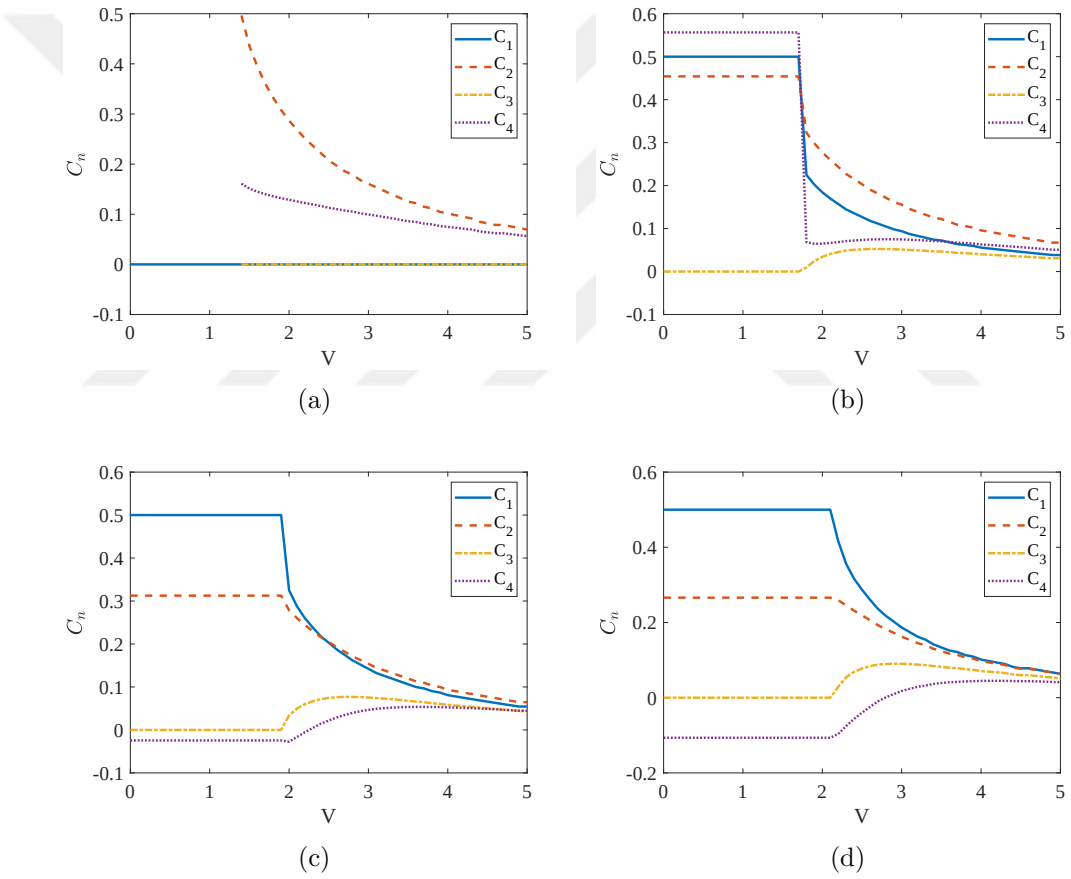

Figure 5.6: First four cumulants as function of V for (a) $\delta = 0$, (b) $\delta = 0.3$, (c) $\delta = 0.5$, (d) $\delta = 0.7$

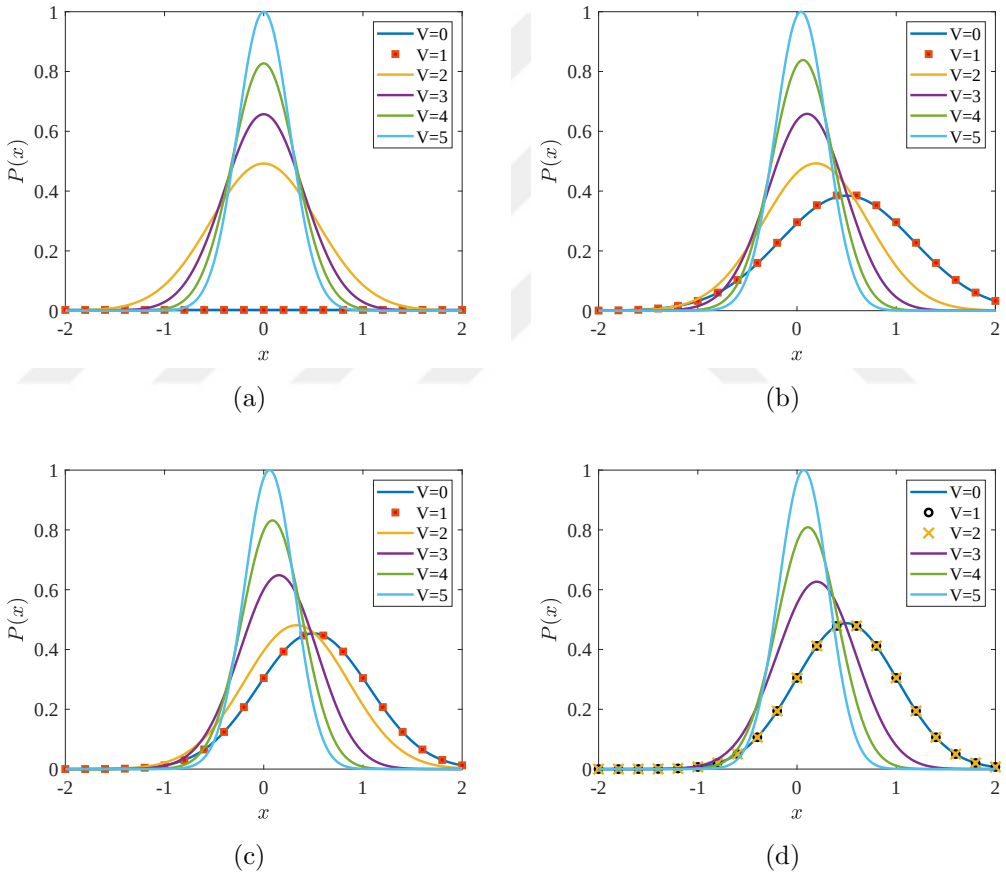

Figure 5.7: Approximate probability distribution for (a) $\delta = 0$, (b) $\delta = 0.3$, (c) $\delta = 0.5$, (d) $\delta = 0.7$

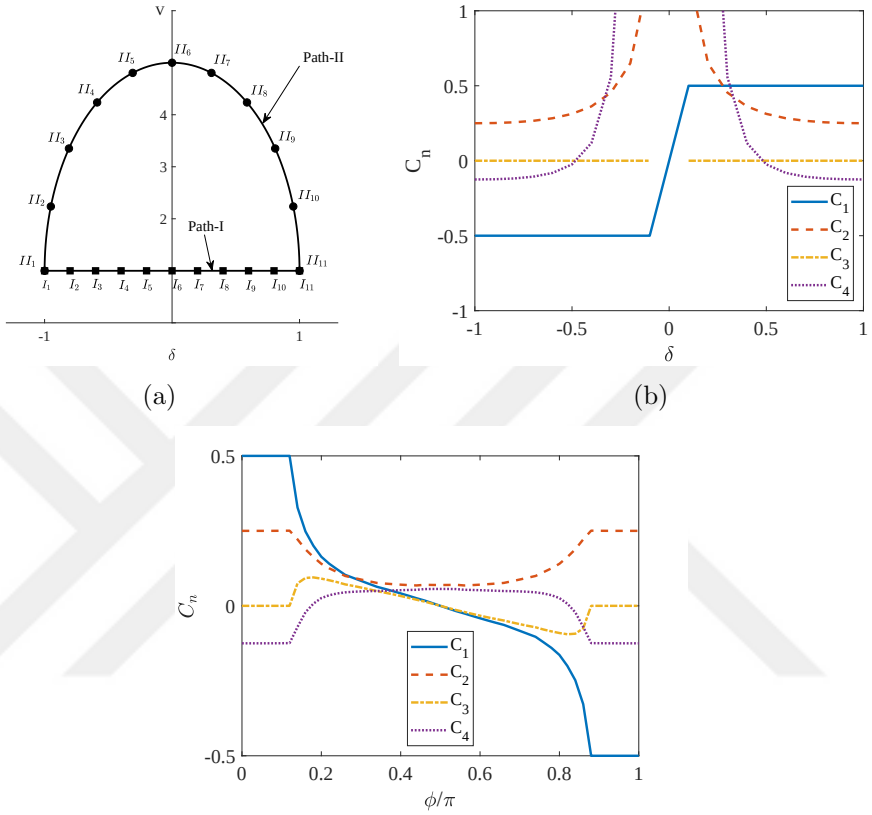

Figure 5.8: (a) Two different paths in parameter space of V and δ, (b) First four cumulants on path-I, (c) First four cumulants on path-II.

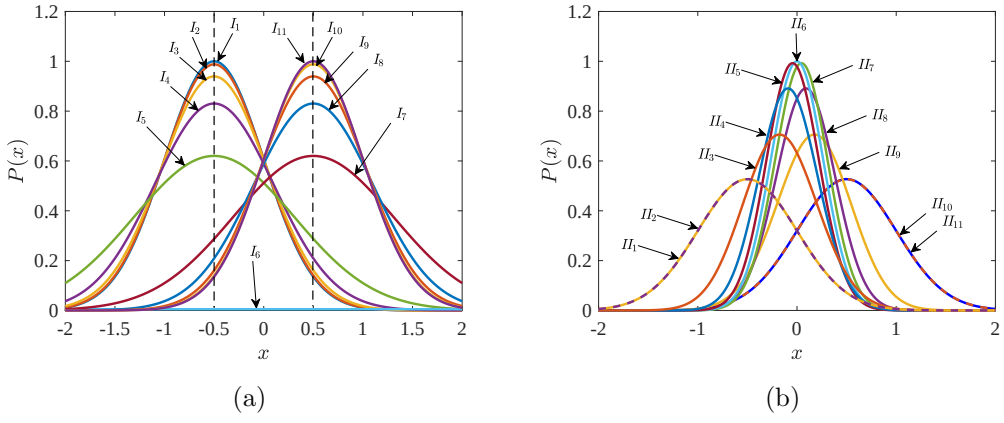

Figure 5.9: Probability distribution on: (a) Path-I, (b) Path-II.

On path-I mean of the probability distribution remain fixed for both $\delta < 0$ and $\delta > 0$ cases. With increase of $|\delta|$ distribution become more localized. It first builds up on $x = -0.5$ and its magnitude decreases with increasing δ from -1 to 0. At $\delta = 0$ probability is a flat line at zero. This state we take as fully delocalized (conducting) state. Further increasing δ build up the probability at other point $x = +0.5$. This sudden jump of distribution shows transportation of one unit of charge from one site to the next. In contrast to this sudden jump of distribution from one site to the next on path-I, on path-II it moves slowly from one site to the next because of interaction. It first builds on $x = -0.5$ with a small magnitude and moves toward zero on which, due to maximum strength of interaction, its magnitude become highest. It ends up on $x = +0.5$ with a symmetric distribution.

It is instructive to calculate polarization distribution of RM model and compare it with distribution of interacting SSH model. One can calculate cumulants of RM model using wave function given by (2.12), (2.14) and (2.19). Take a semi-circular path ($\mathcal{C}$) in the parametric space of δ and Δ where Δ is on-site potential, Figure. 5.10(a). On-site potential breaks the chiral symmetry of SSH model. On this semi-circular path distribution moves slowly form one site to next due to Δ as calculated in Ref. [20]. Distribution is shown in Figure. 5.10(b). It is easy to conclude that interaction has the same effect on SSH model's distribution as on-site potential i.e. it also breaks chiral symmetry. One difference that can be seen between two is that topological non-trivial point of RM become a line in interacting SSH.

By using parent Hamiltonian of interacting SSH model one can trace out the Brillouin zone curves to visualize phase transition. Parent Hamiltonian, given by (3.43), (3.46) and (3.48), can be written as $H_P(k) = \mathbf{h(k)} \cdot \sigma$ where σ are Pauli matrices and $\mathbf{h(k)}$ is 3D vector which traces out closed curve in 3D space of h_x, h_y and h_z. Curves traced out on path-I and II are shown in Figure. 5.11. At $\phi = 0$ (full dimerized limit) $\mathbf{d(k)}$ makes a circle of unit radius and at $\phi = \pi/2$ (metallic phase) it's a straight line on y-axis in (h_y, h_z) plane rather than a curve. In between these values of ϕ, curves resemble to an eclipse which become thinner as ϕ increase. Note that on path-I curves are similar to pseudo-spin vector shown in Figure. 2.2 which shows that system acts like simple SSH phase on this path. On

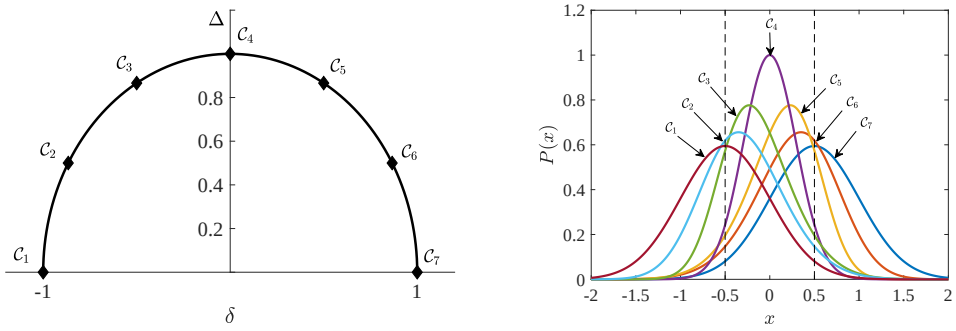

(a) (b)

Figure 5.10: (a) A semi-circular path taken in parametric space of δ and Δ, (b) Approximate probability distribution of RM model on different point of the semi-circular path.

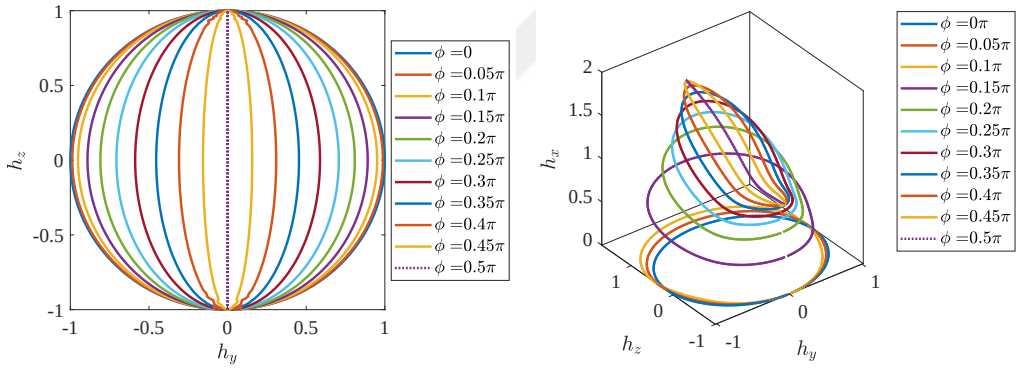

(a) (b)

Figure 5.11: Brillouin zone curves traced out by vector **h(k)** on: (a) Path-*I*, (b) Path-*II*.

path-*II* h_x is non-zero which causes the straight line to move above the (h_y, h_z) plane. It means that on this path there is no gap-closure due to interaction.

Chapter 6

Conclusion

We studied interacting SSH model by extending the variational Baeriswyl wave function to take inhomogeneous hopping between sites into account, numerically calculated phase diagram of the system and studied the polarization probability distribution as a function of interaction. There were three phases found using this variational approximation: SSH, metallic and insulating phase. Phase diagram was quite interesting because for the interacting system we found a metal-insulator transition at $V = 1.3365\ldots$, which is less than exact solution's result ($V = 2$). The phase transition we found was first-order. We also inverted Baeriswyl wave function to get effective parent Hamiltonian. By tracing out the curves of $\mathbf{h(k)}$ vector when k is swiped through Brillouin zone, we visualized phase transition on two different paths.

Study of polarization distribution further explains the effect of interaction on the phase diagram of the model. We calculated the first three cumulants of polarization from which we reconstructed probability distribution using a skewed normal distribution function. It is informative to compare this interacting SSH model's distribution with the distribution of the RM model, which is the SSH model with on-site alternating potential. RM model has a topological non-trivial point (point on which gap closure occurs) at $\delta = \Delta = 0$, where δ is deviation of hopping strength and Δ is on-site potential. When interaction is added in SSH model this topological non-trivial point become a line from $V = 0$ to $V = 1.3365\ldots$. We

reconstruct probability distribution on two different paths in parametric space of δ and V. Both paths connect two different topological states. One path crosses the gap closure line and other path makes an eclipse in space avoiding gap closure line. On the first path, when gap closure line is crossed, distribution changes discontinuously. On the second path, distribution travels slowly from one point to next. This traveling behavior of distribution is also found in the RM model. One can say that turning on the interaction on SSH model gives a symmetry broken state similar to RM ground-state in which symmetry is broken due to alternating on-site potential. One difference that is found between RM and interacting SSH state is that gap closure point of the RM model become a line in interacting SSH model.

Bibliography

[1] S. Rachel and K. Le Hur, "Topological insulators and mott physics from the hubbard interaction," *Phys. Rev. B*, vol. 82, p. 075106, Aug 2010.

[2] C. Griset and C. Xu, "Phase diagram of the kane-mele-hubbard model," *Phys. Rev. B*, vol. 85, p. 045123, Jan 2012.

[3] I. J. Hamad, C. J. Gazza, and J. A. Riera, "Helical currents in metallic rashba strips," *Phys. Rev. B*, vol. 93, p. 205113, May 2016.

[4] M. Hohenadler and F. F. Assaad, "Correlation effects in two-dimensional topological insulators," *Journal of Physics: Condensed Matter*, vol. 25, no. 14, p. 143201, 2013.

[5] M. Laubach, J. Reuther, R. Thomale, and S. Rachel, "Rashba spin-orbit coupling in the kane-mele-hubbard model," *Phys. Rev. B*, vol. 90, p. 165136, Oct 2014.

[6] W. P. Su, J. R. Schrieffer, and A. J. Heeger, "Solitons in polyacetylene," *Phys. Rev. Lett.*, vol. 42, pp. 1698–1701, Jun 1979.

[7] A. J. Heeger, S. Kivelson, J. R. Schrieffer, and W. P. Su, "Solitons in conducting polymers," *Rev. Mod. Phys.*, vol. 60, pp. 781–850, Jul 1988.

[8] R. Jackiw and C. Rebbi, "Solitons with fermion number 1/2," *Phys. Rev. D*, vol. 13, pp. 3398–3409, Jun 1976.

[9] M. C. Gutzwiller, "Effect of correlation on the ferromagnetism of transition metals," *Phys. Rev. Lett.*, vol. 10, pp. 159–162, Mar 1963.

[10] M. C. Gutzwiller, "Correlation of electrons in a narrow s band," *Phys. Rev.*, vol. 137, pp. A1726–A1735, Mar 1965.

[11] K. Yosida, "Bound state due to the $s-d$ exchange interaction," *Phys. Rev.*, vol. 147, pp. 223–227, Jul 1966.

[12] "Electron correlations in narrow energy bands," *Proceedings of the Royal Society of London A: Mathematical, Physical and Engineering Sciences*, vol. 276, no. 1365, pp. 238–257, 1963.

[13] D. S. Rokhsar and B. G. Kotliar, "Gutzwiller projection for bosons," *Phys. Rev. B*, vol. 44, pp. 10328–10332, Nov 1991.

[14] G. Carleo, F. Becca, M. Schiró, and M. Fabrizio, "Localization and glassy dynamics of many-body quantum systems," *Scientific Reports*, vol. 2, pp. 243 EP –, Feb 2012. Article.

[15] K. Ido, T. Ohgoe, and M. Imada, "Time-dependent many-variable variational monte carlo method for nonequilibrium strongly correlated electron systems," *Phys. Rev. B*, vol. 92, p. 245106, Dec 2015.

[16] "Quantal phase factors accompanying adiabatic changes," *Proceedings of the Royal Society of London A: Mathematical, Physical and Engineering Sciences*, vol. 392, no. 1802, pp. 45–57, 1984.

[17] J. Zak, "Berry's phase for energy bands in solids," *Phys. Rev. Lett.*, vol. 62, pp. 2747–2750, Jun 1989.

[18] I. Souza, T. Wilkens, and R. M. Martin, "Polarization and localization in insulators: Generating function approach," *Phys. Rev. B*, vol. 62, pp. 1666–1683, Jul 2000.

[19] Hetényi, Balázs and Yahyavi, Mohammad, "Cumulants associated with geometric phases," *EPL*, vol. 105, no. 4, p. 40005, 2014.

[20] M. Yahyavi and B. Hetényi, "Reconstruction of the polarization distribution of the rice-mele model," *Phys. Rev. A*, vol. 95, p. 062104, Jun 2017.

[21] D. Xiao, M.-C. Chang, and Q. Niu, "Berry phase effects on electronic properties," *Rev. Mod. Phys.*, vol. 82, pp. 1959–2007, Jul 2010.

[22] M. J. Rice and E. J. Mele, "Elementary excitations of a linearly conjugated diatomic polymer," *Phys. Rev. Lett.*, vol. 49, pp. 1455–1459, Nov 1982.

[23] H. Takayama, Y. R. Lin-Liu, and K. Maki, "Continuum model for solitons in polyacetylene," *Phys. Rev. B*, vol. 21, pp. 2388–2393, Mar 1980.

[24] W. P. Su, J. R. Schrieffer, and A. J. Heeger, "Soliton excitations in polyacetylene," *Phys. Rev. B*, vol. 22, pp. 2099–2111, Aug 1980.

[25] J. Ruostekoski, G. V. Dunne, and J. Javanainen, "Particle number fractionalization of an atomic fermi-dirac gas in an optical lattice," *Phys. Rev. Lett.*, vol. 88, p. 180401, Apr 2002.

[26] L. Li, Z. Xu, and S. Chen, "Topological phases of generalized su-schrieffer-heeger models," *Phys. Rev. B*, vol. 89, p. 085111, Feb 2014.

[27] R. Peierls, *More Surprises in Theoretical Physics (Princeton Series in Physics)*. Princeton University Press, 1991.

[28] C. Mora, "Introduction to second quantization,"

[29] C. Kittel, *Introduction to Solid State Physics 7e Im*. John Wiley & Sons Inc, 1996.

[30] J. K. Asbóth, L. Oroszlány, and A. P. Pályi, *A Short Course on Topological Insulators: Band Structure and Edge States in One and Two Dimensions (Lecture Notes in Physics)*. Springer, 2016.

[31] S. A. Jafari, "Introduction to Hubbard Model and Exact Diagonalization," *ArXiv e-prints*, July 2008.

[32] H. Bethe, "Zur theorie der metalle," *Zeitschrift für Physik*, vol. 71, pp. 205–226, Mar 1931.

[33] S. R. White, "Density matrix formulation for quantum renormalization groups," *Phys. Rev. Lett.*, vol. 69, pp. 2863–2866, Nov 1992.

[34] R. Guardiola, "Monte carlo methods in quantum many-body theories," in *Microscopic Quantum Many-Body Theories and Their Applications* (J. Navarro and A. Polls, eds.), (Berlin, Heidelberg), pp. 269–336, Springer Berlin Heidelberg, 1998.

[35] B. Dóra, M. Haque, F. Pollmann, and B. Hetényi, "Quantum quench in two dimensions using the variational baeriswyl wave function," *Phys. Rev. B*, vol. 93, p. 115124, Mar 2016.

[36] *Nonlinearity in Condensed Matter: Proceedings of the Sixth Annual Conference, Center for Nonlinear Studies, Los Alamos, New Mexico, 5–9 May, 1986 (Springer Series in Solid-State Sciences)*. Springer, 2011.

[37] L. G. Molinari, "Notes on Wick's theorem in many-body theory," *ArXiv e-prints*, Oct. 2017.

[38] C. D. Sherrill, "An introduction to hartree-fock molecular orbital theory," 2000.

[39] P. V. Rysselberghe, "Remarks concerning the clausius-mossotti law," *The Journal of Physical Chemistry*, vol. 36, no. 4, pp. 1152–1155, 1931.

[40] R. Resta and D. Vanderbilt, *Theory of Polarization: A Modern Approach*, pp. 31–68. Berlin, Heidelberg: Springer Berlin Heidelberg, 2007.

[41] R. D. King-Smith and D. Vanderbilt, "Theory of polarization of crystalline solids," *Phys. Rev. B*, vol. 47, pp. 1651–1654, Jan 1993.

[42] R. Resta, "Macroscopic polarization in crystalline dielectrics: the geometric phase approach," *Rev. Mod. Phys.*, vol. 66, pp. 899–915, Jul 1994.

[43] K. Bandyopadhyay, A. K. Bhattacharya, P. Biswas, and D. A. Drabold, "Maximum entropy and the problem of moments: A stable algorithm," *Phys. Rev. E*, vol. 71, p. 057701, May 2005.

[44] R. Collins and A. Wragg, "Maximum entropy histograms," *Journal of Physics A: Mathematical and General*, vol. 10, no. 9, p. 1441, 1977.